Glacier expansion in central Patagonia during the Antarctic Cold Reversal followed by retreat and stabilisation during the Younger Dryas

Glacier expansion in central Patagonia during the Antarctic Cold Reversal followed by retreat and stabilisation during the Younger Dryas

Monika Mendelová[a,*], Andrew S. Hein[a], Ángel Rodes[b], Rachel K. Smedley[c], Sheng Xu[b]

[a] *University of Edinburgh, School of Geosciences, Drummond Street, Edinburgh, EH8 9XP, UK*
[b] *Scottish Universities Environmental Research Centre, Scottish Enterprise Technology Park, East Kilbride, G75 OQF, Glasgow, UK*
[c] *University of Liverpool, Department of Geography and Planning, Chatham Street, Liverpool, L69 7ZT, UK*

Abstract

The spatial-temporal footprint of millennial-scale climate events during the last glacial-interglacial transition can yield insights into the underlying drivers of climate change, but remains poorly resolved in Patagonia. Here, we assess the glacier response to abrupt cold events and palaeolake evolution using geomorphological mapping along with ^{10}Be ages and optically stimulated luminescence ages from near Lago Belgrano (47.9° S) on the eastern side of Monte San Lorenzo. The former Belgrano glacier was sustained by a climatically sensitive ice cap, making the site ideal for investigating the glacier response to abrupt cold reversals. Our data reveal an extensive re-advance at 13.1 ± 0.6 ka, consistent with cooling and increased precipitation during the Antarctic Cold Reversal (ACR). Subsequently, ice retreated by

*Corresponding author
Email address: m.mendelova@sms.ac.uk (Monika Mendelová)

at least 10 km and created an ice-dammed proglacial lake in the Belgrano valley. Rapid recession was punctuated by smaller advances/still-stands sufficient to maintain an ice-dam for the palaeolake and deposit a lateral moraine dated at 12.4 ± 0.3 ka during the Younger Dryas (YD). The final withdrawal of glaciers to the mountains allowed the palaeolake to drain and resulted in an Atlantic/Pacific drainage reversal. This marks the final separation of the Patagonian Ice Sheet into the individual ice fields at the YD-Holocene transition. Our data demonstrate the dominant ACR climate signal in central Patagonia, but also reveals a co-occurrence of the northern hemisphere YD signal, albeit of smaller magnitude. The ACR re-advance was primarily climatically controlled, but its relative magnitude was likely a consequence of ice divide migration and ice flow re-routing during the break-up of the Patagonian Ice Sheet.

Keywords:

South America, Quaternary, Antarctic Cold Reversal, Younger Dryas, Cosmogenic isotopes, Luminescence dating, glacial geomorphology, glaciology

---

1. Introduction

The last glacial-interglacial transition (LGIT, 18 - 11 ka) was characterized by the demise of ice-sheets, reorganization of the atmospheric and oceanic systems accompanied by increasing atmospheric CO^2, and millennial-scale warm/cold events (Denton et al., 2010). The interhemispheric phasing of climate change during this period has generated much debate, in particular the occurrence of the Antarctic Cold Reversal (ACR; $\sim$ 14.6 - 12.8 ka, Lemieux-Dudon et al., 2010) and the northern hemisphere Younger Dryas (YD; $\sim$ 12.9 - 11.7 ka; Blunier et al., 1998) climate signals in the southern hemisphere (e.g. Denton et al., 1999; Sugden et al., 2005; McCulloch et al., 2005; Putnam et al., 2010a; Glasser et al., 2012). The relative magnitude and the spatial-temporal footprint of these abrupt events can yield insights into the processes involved in initiation and propagation of climate change, but remains poorly resolved in Patagonia.

Patagonia is well-situated for studying this as it intersects the Southern Westerly Winds (SWW), which modulate the global carbon cycle, exert a strong influence on Southern Ocean circulation, and which played an important role in the LGIT by controlling atmospheric CO^2 (Lamy et al., 2007; Toggweiler et al., 2006; Anderson et al., 2009; Marshall and Speer, 2012). The global climate models predict a poleward shift and strengthening of the SWW in the future, yet also show considerable spatial variability in the magnitude of the strength and position change (Meijers, 2014). Better constraining the timing and magnitude of past glacier fluctuations along latitudinal gradients in the southern mid-latitudes can help to improve our understanding of past climate change, including the role of the SWW, and can help to improve projections of future climate change. Further, examining the consequences of the past rapid climate events on the terrestrial environments, including the cryospheric component, is important for contextualizing present and future climate change in the region.

In Patagonia, the ACR signal is well-documented south of 50° S by both glacier chronologies and palaeovegetation records, which reveal glacier advances and cooling coeval with the ACR (Mansilla et al., 2016; Moreno et al., 2012; Björck et al., 2012; García et al., 2012; Moreno et al., 2009; Fogwill and Kubik, 2005; Strelin et al., 2011; Kaplan et al., 2011; Ackert et al., 2008; Sugden et al., 2005; McCulloch et al., 2005). Here, subsequent ice retreat and warming was interrupted by stabilisation of glaciers during the YD (Kaplan et al., 2011; Moreno et al., 2009). North of 50° S, the glacier response to climate during the LGIT remains poorly resolved. Glacier advances/still-stands during the ACR (Sagredo et al., 2018; Davies et al., 2018; Nimick et al., 2016) as well as YD (Sagredo et al., 2018; Glasser et al., 2012; Nimick et al., 2016) have been reported east of the Northern Patagonian Icefield and on the north-western flanks of Monte San Lorenzo. Many of these glaciers calved into a large regional palaeolake during most of the LGIT (Davies et al., 2018; Thorndycraft et al., 2019), and this process together with topographic pinning points on the ice bed likely exerted a strong influence on their dynamics and response to cold reversals (Davies et al., 2018). In addition, many exposure ages from moraine boulders previously interpreted as dating YD advances (Glasser et al., 2012), are considered erroneously young as a consequence of their submergence in a palaeolake (Thorndycraft et al., 2019). In some cases, the relationship between the dated moraines (e.g. Nimick et al., 2016) and palaeolakes remains unclear. Where YD moraines have been dated, they are based on a limited number of exposure ages ($\leq$ 2) (Sagredo et al., 2018; Glasser et al., 2012). Thus, firm dating of YD ice limits has not yet been achieved.

Terrestrial palaeovegetation proxies from central Patagonia (49° S - 44° S) either: (i) do not document any clear changes from which an ACR or YD signal can be inferred (Haberle and Bennett, 2004; Bennett, 2000; Lumley and Switsur, 1993; Markgraf et al., 2007; de Porras et al., 2014, 2012; Iglesias et al., 2016), or (ii) suggest persistence of cold/cool and wet conditions from about 16 ka to 11.8 ka (Villa-Martínez et al., 2012). Only one terrestrial record so far suggests increased precipitation coeval with the ACR, based on an increase of cold-resistant hygrophilous taxa between 14 ka and 13.5 ka (Henríquez et al., 2017). This is supported by pollen analysis on a marine core recovered from offshore of Chile (46° S; MD07-3088, Montade et al., 2013). The absence of the ACR and/or YD signal in many records might be masked by high climate variability during the LGIT , combined with the effects of local climate and/or insensitivity of proxies to minor cooling (Markgraf et al., 2007; Villa-Martínez et al., 2012; Mendelova et al., 2017).

The aim of this study is to assess the glacier response to cold reversals during the LGIT in the Belgrano and Lacteo valleys on the eastern side of Monte San Lorenzo. We selected this site because the relatively small San Lorenzo ice cap would have been more sensitive to climate change than the larger Patagonian icefields. At its maximum extent during the LGIT, the former Belgrano glacier had a land-terminating margin rather than a calving margin, and thus glacier fluctuations here are more likely to reflect changes in climate. These characteristics make the site ideal for investigating the regions glacier response to abrupt millennial-scale cooling events during the LGIT. We use geomorphological mapping, cosmogenic ^{10}Be surface exposure dating and optically-stimulated luminescence (OSL) analysis to determine the timing of 1) major glacier re-advances/stillstands during the LGIT, and 2) the formation and evolution of palaeolakes in the valleys. Our mapping and chronology gives insight on the processes involved in the break-up of the former Patagonian Ice Sheet (PIS) and rates of deglaciation.

2. Study area and previous work

2.1. Physical setting

Monte San Lorenzo (3706 m, Chilean name: Monte Cochrane) is an isolated massif located $\sim$ 80 km east of the main spine of the Patagonian Andes (Figs. 1 and 2). At this latitude, the main chain of the Andes exhibits a tectonic depression, which separates Monte San Lorenzo massif from the Pacific coast, and the Northern Patagonian Icefield from the Southern Patagonian Icefield. The Lago Belgrano valley is a relatively small, low gradient, high elevation valley at over 850 m asl. This contrasts with the large overdeepened basins to the north and south (e.g. Lago Puyerredón, 150 m) that have been eroded to below sea level (Murdie et al., 1998). The low gradient Belgrano valley also contrasts with mountain valleys on the northern and western flanks of Monte San Lorenzo, which have steeper elevation profiles as they descend to low elevations ($\sim$ 500 - 200 m asl) within tens of km of the mountain. San Lorenzo is part of the Patagonian Batholith intrusion (Ramos and Kay, 1992; De Arellano et al., 2012), and is the main source of granitic erratics that are found in the Belgrano valley.

The precipitation-bearing SWW have a dominant influence on climate and sustain the present day ice-fields and glaciers. Westerly precipitation can reach 5,000 - 10,000 mm a^{-1} on the western side of the Andes and falls to less than 300 mm a^{-1} tens of km downwind of the mountain front (Garreaud et al., 2013). As a consequence of the topographic depression, the Monte San Lorenzo massif is the first orographic barrier to the SWW, and

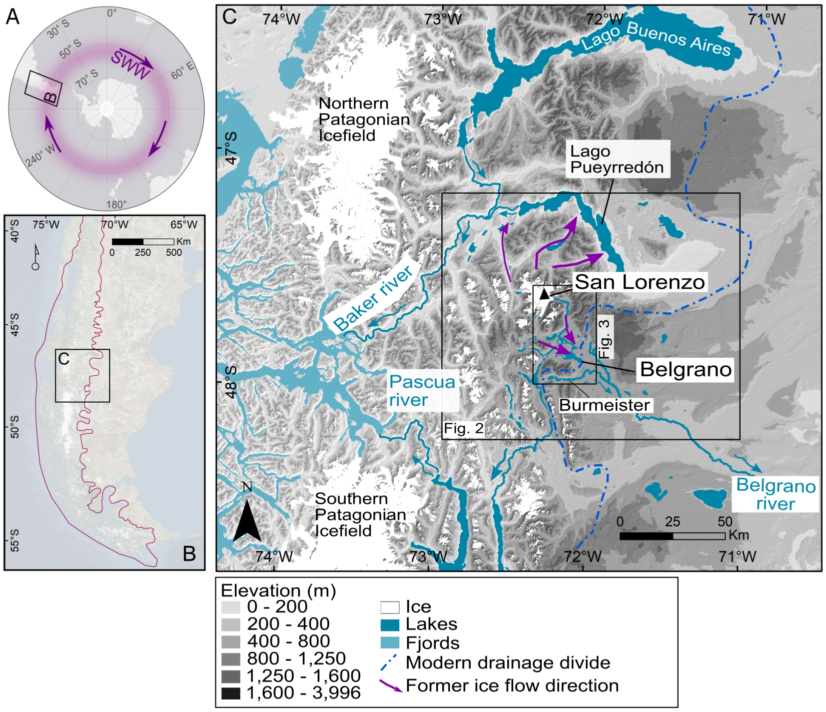

Figure 1: A) Location of Patagonia in the southern hemisphere with approximate location of the Southern Westerly Winds. B) Location of the study area in Patagonia, with an approximate extent of the Patagonian Ice Sheet at the global Last Glacial Maximum (pink line). Image: ESRI World Imagery. C) Map of central Patagonia showing contemporary ice fields and ice caps (outlines were downloaded from the GLIMS database (Falaschi et al., 2017; De Angelis et al., 2015)), modern drainage divide and location of Monte San Lorenzo and Lago Belgrano valley. Magenta arrows indicate former ice discharge routes from the San Lorenzo. Basemap: Shuttle Radar Topography Mission DEM.

has a transitional maritime to continental climate (Falaschi et al., 2013).

The San Lorenzo massif sustains four valley glaciers and several smaller ice bodies covering a total area of $\sim$ 139 km^2 (Falaschi et al., 2013). The snowline is estimated to be $\sim$ 1700 - 1750 m a.s.l on the western side and about 100 m higher on the eastern side of the massif (Falaschi et al., 2013).

All glaciers of the San Lorenzo massif and Lago Belgrano drain westward to the Pacific Ocean via rivers, which exploit the gap in the mountain chain (Fig. 2). The drainage divide is located east of Lago Belgrano, and Lago Burmeister ($\sim$ 900 m asl; Fig. 2) is over the divide and instead drains eastward to the Atlantic Ocean via the Río Belgrano. During glacial cycles, the build-up of ice along the Andean mountain chain blocked Pacific drainage pathways, causing large-scale drainage reversals. The break-up of the Patagonian Ice Sheet is thus associated with large-scale drainage reversals across many parts of Patagonia (Caldenius, 1932; Turner et al., 2005; Thorndycraft et al., 2019).

2.2. Previous work

During full glacial conditions, the San Lorenzo ice cap coalesced with the larger PIS (Caldenius, 1932; Wenzens, 2005; Glasser et al., 2005; Mendelova et al., 2019). Ice from the San Lorenzo centre discharged northwards to join the Lago Puyerredón outlet glacier and south-eastwards into the Belgrano valley (Fig. 1 C; Wenzens, 2002). The Belgrano glacier had additional ice contribution from accumulation areas on the mountains to the west and south of Lago Belgrano.

Following disintegration of the Lago Puyerredón lobe, ice on the northern and western flanks of San Lorenzo was largely confined to the mountain valleys (Davies et al., 2018; Martin et al., 2019; Sagredo et al., 2018). Here, advances of the Tranquilo and Calluqueo glaciers were dated at 13.8 $\pm$ 0.5 ka and 13.2 $\pm$ 0.2 ka, respectively, coeval with the ACR (Fig. 2; Sagredo et al., 2018; Davies et al., 2018). At this time, the Calluqueo glacier calved into a palaeolake, and part of the moraine was subaqueous (Davies et al., 2018). YD stabilisation is suggested by a couple of exposure ages from inset moraines in both valleys (Fig 2; 12.5 ± 0.4 and 11.6 ± 0.4 ka in the Tranquilo valley (Sagredo et al., 2018), and 12.9 ± 0.8 and 12.0 ± 0.5 in the Salto valley (Glasser et al., 2012)).

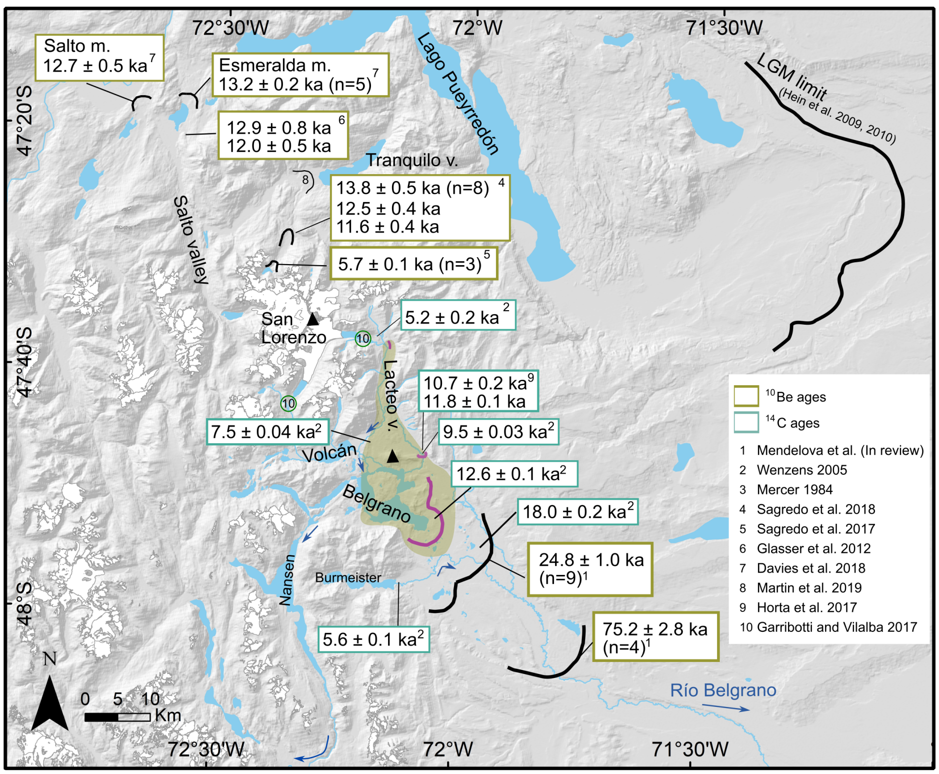

Figure 2: Map showing Monte San Lorenzo, Lago Belgrano and Lacteo valleys, along with published chronologies (black curves indicate dated ice margins). Where more than 2 ages exist for a landform, uncertainty-weighted means with 1 σ standard deviation are presented. Otherwise, individual ages are given with 1 σ uncertainty (internal in case of ^{10}Be ages). Green shading indicates our study area, and ice margins dated in this study are highlighted in pink. Glacier outlines were downloaded from the GLIMS database (Falaschi et al., 2017; De Angelis et al., 2015). River drainage directions are indicated with blue arrows.

The Belgrano glacier reached its full last glacial extent at 75.0 ± 2.8 ka based on ^{10}Be exposure ages from outwash cobbles (Fig. 2; Mendelova et al., 2019). This early maximum suggests that an independent ice mass developed on San Lorenzo early in the last glacial cycle toward the end of MIS 5. A second major advance deposited the Menelik moraines dated using ^{10}Be ages at 24.7 ± 1.0 ka (Fig. 2; Mendelova et al., 2019), coeval with the global Last Glacial Maximum (gLGM).

The Late Glacial history at Lago Belgrano is only constrained by two minimum radiocarbon ages of 12.6 ± 0.06 cal ka BP and 9.5 ± 0.04 cal ka BP (Wenzens, 2005; Table 1 and Fig. 2). With the exception of the Tranquilo valley, where Sagredo et al. (2018) dated an advance to 5.7 ka ± 0.1 ka using ^{10}Be, our knowledge of the Holocene dynamics of the San Lorenzo glaciers is limited to minimum radiocarbon ages and lichenometry (Garibotti and Villalba, 2017; Mercer, 1984; Wenzens, 2005). In the Lacteo valley (Fig. 2), Wenzens (2005) obtained an age of 7.5 ± 0.04 cal ka BP from a kettle hole, and further up valley, Mercer (1984) obtained a maximum age of 5.2 ± 0.2 cal ka BP from an overridden tree incorporated within a moraine 5 km from the present day margin of the Lacteo glacier. Wenzens (2005) obtained a minimum age of 5.6 ± 0.06 cal ka BP from a kettle hole within the moraines bounding Lago Burmeister (Fig 2). Horta et al. (2017) proposed a palaeolake in the Belgrano valley at 900 - 920 m a.s.l. between 11.7 and 10.8 ka on the basis of two radiocarbon ages from lacustrine deposits (Table 1 and Fig 2).

Geomorphological mapping of the valleys on the eastern side of Monte San Lorenzo along with a robust chronology will allow us to assess the response of this small ice cap to climate fluctuations during the ACR and YD, and will provide insight on the overall pattern and rate of deglaciation.

3. Methods

In this study, we focus on a moraine system that bounds the eastern end of Lago Belgrano, here informally named the Belgrano moraine system, and the area to the north, including the Lacteo valley (Figs. 2 and 3). The two older moraine systems in the Belgrano valley (Fig. 2) and associated chronologies are described by Mendelova et al. (2019).

Geomorphological mapping was done from high resolution optical satellite imagery (2.5 m to sub-meter) distributed by the ESRI^{TM} World Imagery service, 10 m Sentinel-2 imagery and Google Earth. ALOS PALSAR (12.5 m) and Shuttle Radar Topography Mission (30 m) digital elevation models were used to aid landform identification. Geomorphological features were mapped following established criteria (e.g. Glasser et al., 2008; Darvill et al., 2014; Bendle et al., 2017; Martin et al., 2019). Mapping was field-checked during two field campaigns in 2016 and 2018.

Published ^{10}Be ages from Patagonia described in this paper were recalculated using the protocol outlined in section 3.1.2, and ages are presented as uncertainty (internal) weighted means with 1 σ standard deviation per moraine. Published radiocarbon ages (Table 1) were recalibrated using the OxCal online calibration program (version 4.3; Bronk Ramsey, 2009) and the southern hemisphere calibration curve (SHCal13, Hogg et al., 2013). The calibrated median ages (95.4 % confidence interval) are presented as "cal. ka BP", rounded to the nearest 100 a.

3.1. Surface exposure dating

3.1.1. Sampling

For cosmogenic nuclide analysis, we collected samples from the top centre of large boulders embedded in the moraine crests using hammer and chisel (Gosse and Phillips, 2001; Darvill, 2013). We targeted granitic boulders that showed minimal surface erosion, and appeared stable. We sampled four to six boulders per moraine limit (cf. Putkonen and Swanson, 2003). Three samples were collected from boulders and cobbles deposited atop bedrock outcrops along a transect in the Lacteo valley to date deglaciation of the valley. Additionally, we collected two surface samples from beach gravels on former shorelines. The shoreline samples consisted of an amalgamation of 30-40 quartz-rich pebbles (2-4 cm).

Sample locations were recorded with a handheld Garmin GPS with a reported accuracy of 3 - 5 m. Topographic shielding was measured in the field using a compass and clinometer, and shoreline altitudes were cross-checked with a barometric altimeter. Sample details are presented in Table 2 and sample locations are shown in Figure 3.

The samples were crushed whole, except sample RV1609, which was cut horizontally to reduce its thickness. Subsequently, the samples were sieved to obtain the sand fraction and then prepared as ^{10}Be AMS targets at two different cosmogenic nuclide laboratories: the Natural Environment Research Council's Cosmogenic Isotope Analysis Facility (NERC-CIAF), and the University of Edinburgh's Cosmogenic Nuclide Laboratory. All Accelerator Mass Spectrometry (AMS) measurements were conducted at the Scottish Universities Environmental Research Centre (SUERC) AMS Facility. Sample preparation for cosmogenic nuclide analysis is described in Mendelova et al. (2019).

3.1.2. Age calculations

^{10}Be ages were calculated using the online exposure age calculator described by Balco et al. (2008), version 3, with a local ^{10}Be production rate for Patagonia (Kaplan et al., 2011), derived from the ICE-D online database (`http://calibration.ice-d.org/`). Ages presented here (Table 3) use the time-dependent Lm scaling scheme of Lal (1991) modified by Stone (2000). The ages decrease by 0.5 % if calculated using the New Zealand production rate of Putnam et al. (2010b) and decrease by 6% with the global production rate of Borchers et al. (2016). Summary statistics for each moraine are given in Table 3. We base our discussion on the uncertainty-weighted means and 1 σ standard deviation.

No correction is applied for shielding by vegetation or snow because the moraines are sparsely vegetated by grasses with the exception of some Nothofagus trees scattered on the lateral moraines in the Lacteo valley. Given high winds and low precipitation, we expect the snow cover to be minimal and short-lived in the Belgrano valley. Closer to the mountain front, snow cover would be more persistent, but boulders perched on moraines are likely to sit above the snowpack where they can be blown free of snow. Exposure ages assume zero erosion, although rates of 0.2 mm ka^{-1} have been estimated nearby (Hein et al., 2017; Douglass et al., 2007). Including this rate would increase ages by less than 1%, which is within analytical uncertainties.

The moraine boulder ages are interpreted to date moraine stabilisation following ice withdrawal, and thus the ages provide a minimum age for the ice advance. The cosmogenic nuclide ages are considered minimum ages, given the potential for post-depositional processes (e.g. erosion and exhumation of boulders) that could affect surface exposure. That said, we acknowledge inheritance could interfere with this assumption, and this is discussed explicitly.

The exposure ages from shorelines are interpreted to date the abandonment (stabilisation) of the shoreline, and therefore dropping of the lake level. We assume that wave action cuts into existing sediment and subjects individual clasts to surface erosion such that inheritance is negligible. This assumption is, however, difficult to test without several samples from each shoreline. Our approach of amalgamating many surface clasts should go some way toward minimising the influence of inheritance on the final ^{10}Be concentration of the sample.

3.2. OSL dating

We collected two samples for luminescence dating from laminated silt and sand sediments interpreted as glaciolacustrine deposits. We interpret the ages to date the deposition of these sediments, and they should therefore give a minimum age for the development of a palaeolake.

Samples for luminescence dating were collected in opaque tubes and prepared for analysis under subdued lighting conditions following the procedure of Smedley et al. (2016). To calculate the environmental dose-rate throughout burial for each sample, U, Th and K concentrations were measured for $\sim$ 80 g of the bulk sediment sample using high-resolution gamma spectrometry. Environmental dose-rates determined for samples RV1801 (212 - 250 μm) and LBSH1801 (125 - 180 μm) are shown in Table S1. Coarse grains of K-feldspar were used to determine equivalent doses (D_e) using 300 μm-diameter single-grain discs and a Risø TL/OSL DA-15 automated single-grain system equipped with a $^{90}Sr/^{90}Y$ beta source (Bøtter-Jensen et al., 2003). Single aliquot regenerative dose (SAR) protocols (Murray and Wintle, 2000) were used for the post-IR IRSL analyses performed at 225 °C (Thomsen et al., 2008), termed the pIRIR$_{225}$ signal. Grains from both samples were used for dose-recovery experiments and successfully recovered a given dose within 10 % using the pIRIR$_{225}$ signal. Fading experiments reported g-values of -0.4 ± 0.7 %/decade (RV1801) and -1.0 ± 0.7 %/decade (LBSH1801), which suggests that no fading correction was required for the pIRIR$_{225}$ signal. D_e values were calculated from all grains passing all the screening criteria. The minimum age model (MAM; Galbraith et al., 1999; Galbraith and Laslett, 1993) was applied to determine an age for the samples as the asymmetrical D_e distributions suggested the samples were partially bleached prior to burial (Fig. S1). The D_e values were then divided by the environmental dose-rates to determine an age for each sample (Table S1). See the supplementary material for full details on the luminescence dating in this study.

4. Results

4.1. Geomorphology

The Belgrano moraine system (Figs. 4 and 5) is comprised of up to 10 arcuate moraine ridges with undulating crests. The outermost moraine ridge is subdued at 3 m height and a slope of 5°. The morphology of this moraine ridge may indicate that the glacier occupied this position for a shorter time or the moraine ridge degraded post-deposition. The next two moraine ridges are the most prominent and continuous with about 10 m in height and slopes up to 22°. Inboard of these the moraines appear more hummocky with occasional inter-morainic depressions. The inner moraine ridges are again distinct with 10 m in relief. The moraines are vegetated by grasses and short shrubs with patches of exposed coarse gravel and large cobbles. We sampled four boulders on the innermost moraine ridges, and four boulders on the outermost subdued moraine ridge (Fig. 4). A broad glaciofluvial outwash plain grades from the moraines toward the east with preserved braided channels.

The Belgrano moraines cross-cut older recessional moraines (cf. Mendelova et al., 2019) on the northeastern side of the lake (Figs. 5 and 6), indicating that the Belgrano moraines were deposited by a re-advance of the Belgrano glacier, rather than a still-stand during overall deglaciation. The location of the older recessional moraines suggest that after the culmination of the gLGM advances/still-stands, the Belgrano glacier withdrew and was largely confined to its trough prior to the re-advance.

To the north of the Belgrano moraines exists a series of latero-terminal moraines (Fig. 5), here informally termed the Rincon moraines, which were deposited by the Lacteo glacier. The Rincon moraines occupy the same morphostratigraphic position as the Belgrano moraines. They are situated on the northern slope of Monte Leon and in the gap between Monte Leon and the NE valley side. The terminal moraine ridges (Figs. 7 A and B) are discontinuous and have been dissected by several meltwater channels up to 40 m in width. We collected four ^{10}Be samples from the terminal moraine ridges. A glaciofluvial outwash grades from the moraines toward the southeast, extending for about 6 km until it merges with the Belgrano outwash. Immediately outboard of the Rincon moraines, the outwash terrace

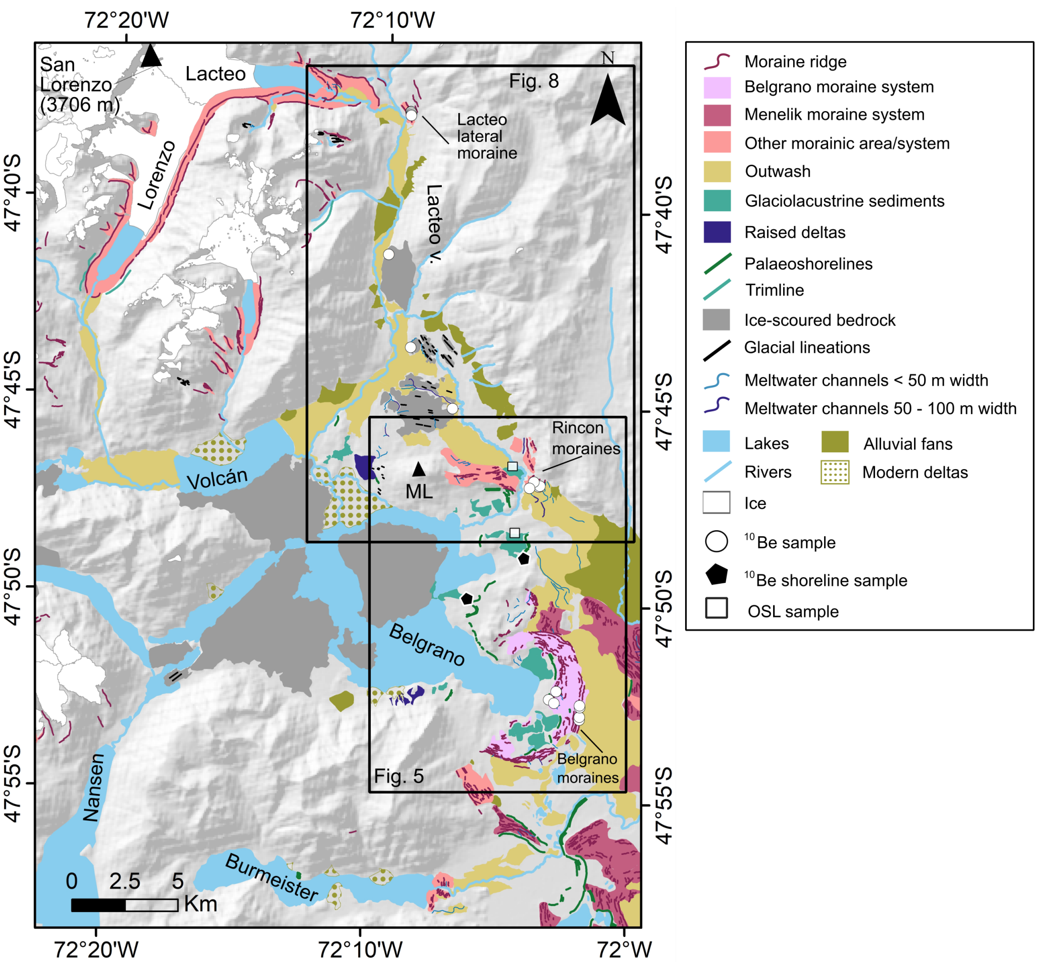

Figure 3: The geomorphological map of the Belgrano and Lacteo valleys. Sample locations are also shown (white circles). The hillshade basemap was derived from the Shuttle Radar Topography Mission Digital Elevation Model.

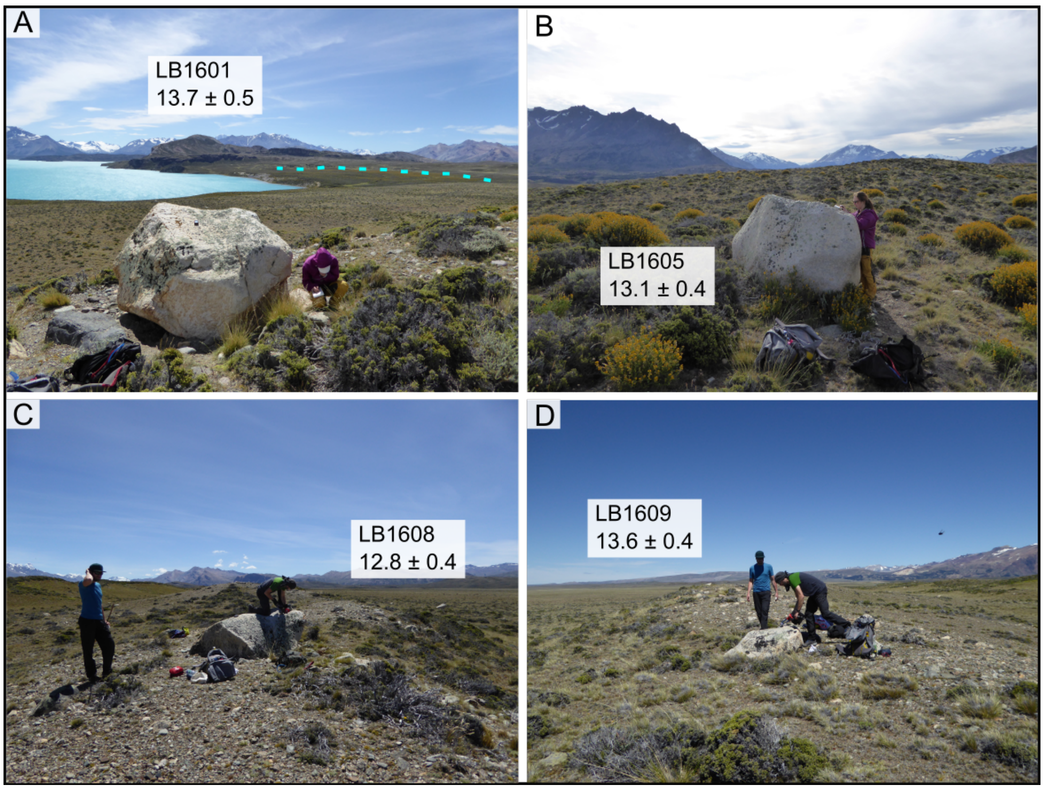

Figure 4: Examples of moraine boulders sampled for surface exposure analysis. (A & B) Boulders on the innermost Belgrano moraine, a former shoreline is visible in the background (A, dashed line). (C & D) Boulders on the outermost Belgrano moraine.

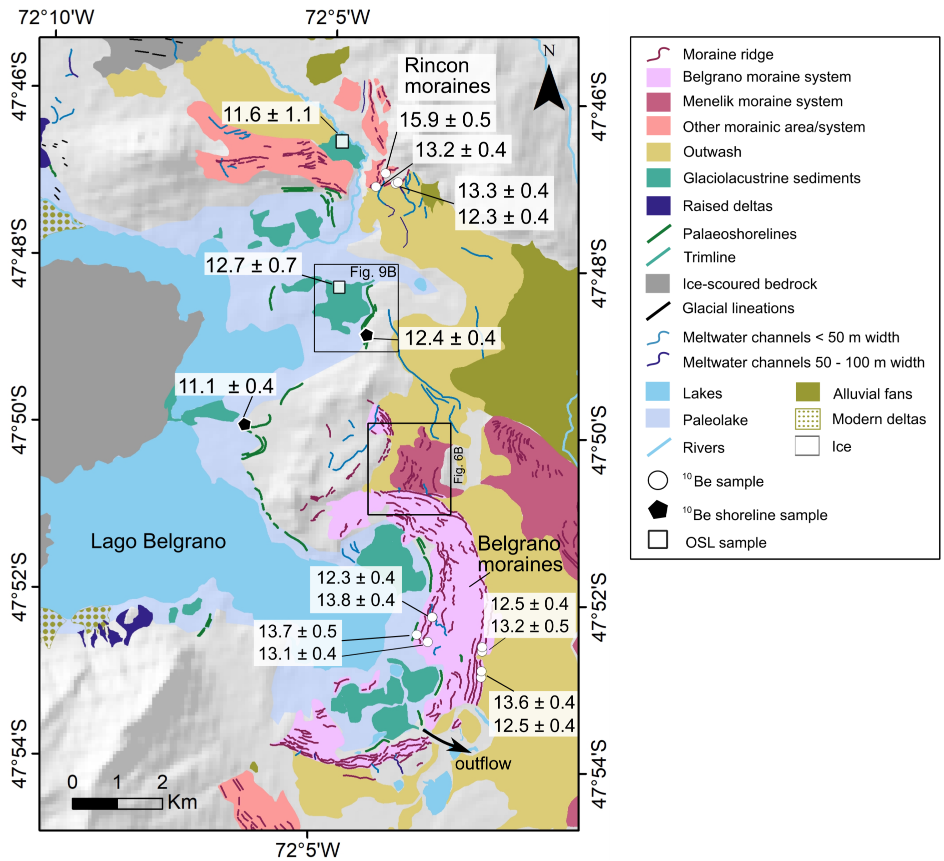

Figure 5: Enlarged geomorphology map showing the Belgrano and Rincon moraines. The locations of moraine boulder samples, shoreline samples and OSL samples collected from glaciolacustrine deposits are also shown. The area where the Belgrano moraines cross-cut older recessional moraines is indicated with a box (Fig.6 B). The ^{10}Be ages presented here are individual ages with 1 σ internal uncertainty. The approximate area of the palaeolake is indicated. This is based on 882 m asl elevation extracted from an SRTM DEM with resolution of 30 m.

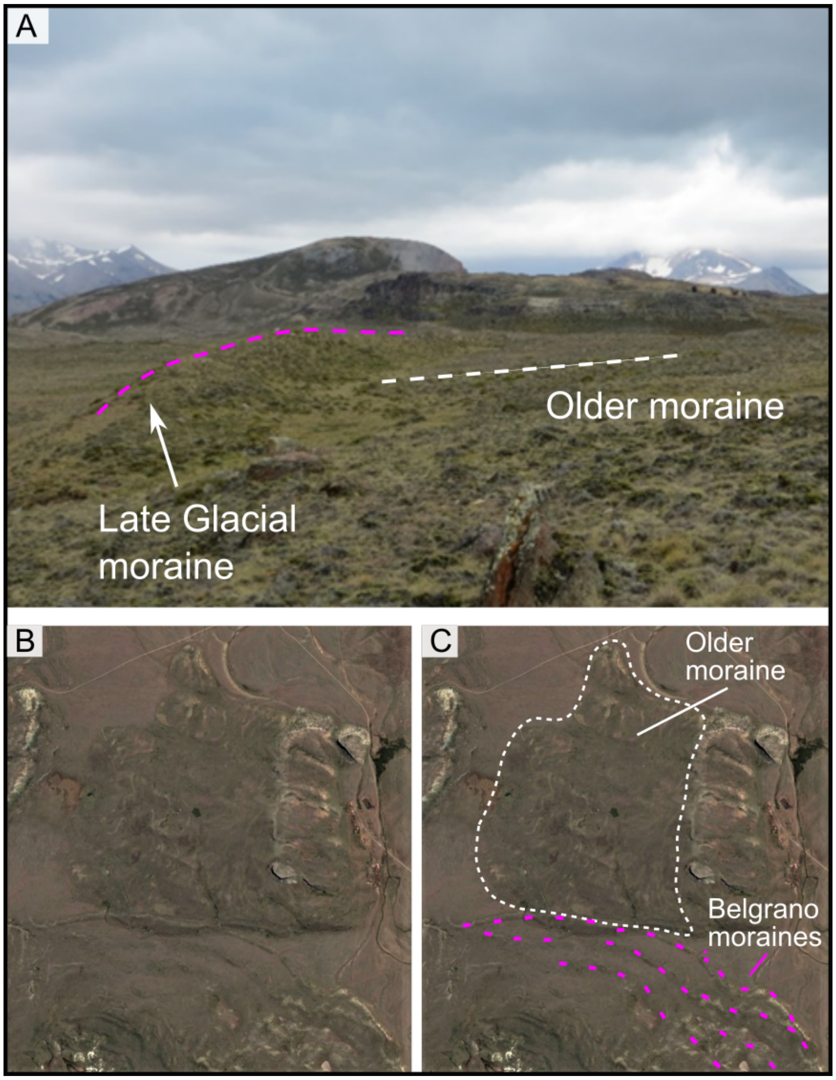

Figure 6: (A) Photograph showing the area where the Belgrano moraines cross-cut older moraines. (B & C) Satellite images showing the cross-cutting relationship (Image: Google Earth).

has been incised by meltwater channels creating a series of stepped terraces.

About 20 km upvalley from the Rincon moraines, and 7 km from the present day margin of the Lacteo glacier, there is a prominent multi-crested lateral moraine perched 45 - 60 m above the valley floor (Fig. 8). This lateral moraine spans a width of 100 m with several distinct crests (2-5 m in relief) that are rich in surface boulder (Figs. 7 C & D). Given that the lateral moraine is only 45 - 60 m above the valley floor, we interpret the moraine to be morphostratigraphically younger than the Rincon moraines. We collected six ^{10}Be samples from this lateral moraine.

4.1.1. Palaeo shorelines

A major palaeo-shoreline at 882 - 885 m asl can be traced along the southern and northern shores of Lago Belgrano and on the ice-proximal side of the Belgrano moraines (Figs. 5 and 9). This shoreline is most prominent on the eastern end of the lake where wave action from westerly winds would have been at its greatest. Here, the shoreline is etched into bedrock and sediment, but traces of the shoreline were observed at least 10 km upvalley, and thus the lake covered a substantial area. Higher shorelines can also be found (e.g. at $\sim$ 889 - 892 m asl.), but are spatially restricted, and could indicate a higher palaeolake level or smaller ice-marginal lakes.

The palaeolake drained eastward to the Atlantic via an outflow through the Belgrano moraines at $\sim$ 883 m asl (Fig. 5). The palaeolake Belgrano existed when the drainage route through to Lago Nansen (Fig. 2) was blocked by ice. The lowering of the lake indicates the loss of this ice dam, and the retreat of ice back into the high mountains. Sediment from this lake, mainly laminated silt to sandy-silts, are preserved at several locations throughout

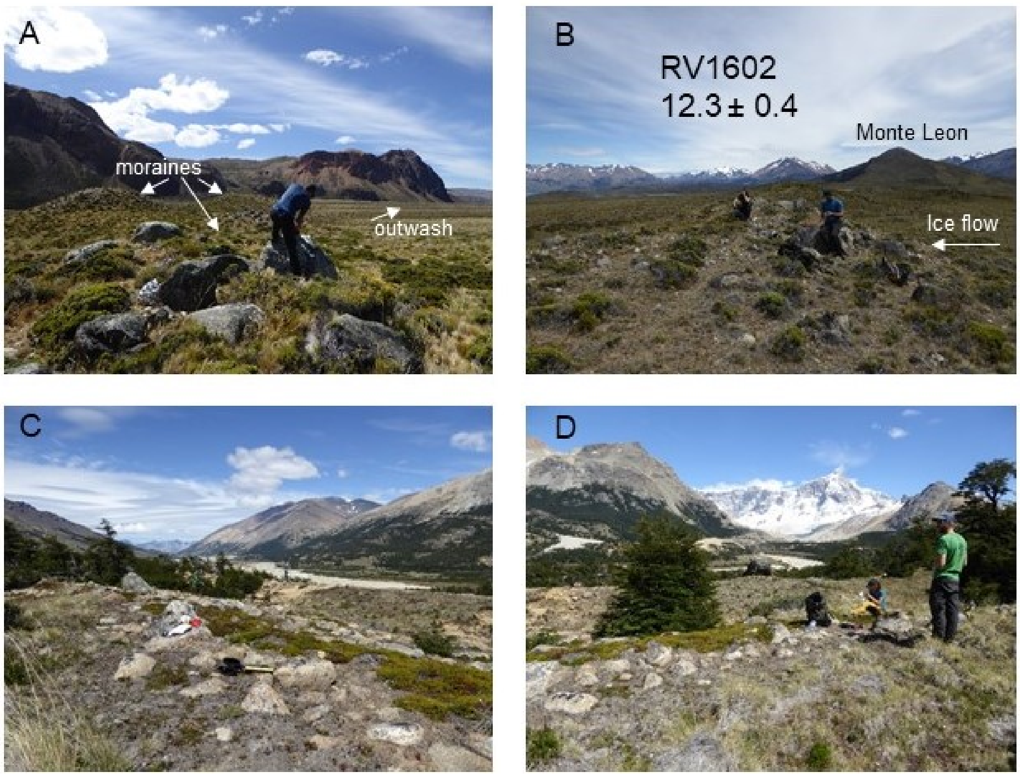

Figure 7: (A & B) Photographs showing the Rincon moraines and an outwash plain grading from the moraines to the SE. The outwash terrace was incised by meltwater creating a series of stepped terraces. (C & D) Photographs showing the multi-crested lateral moraine in the Lacteo valley, about 7 km from the present day margin of the Lacteo glacier.

the basin. We collected two ^{10}Be samples from the 882 - 885 m asl shorelines (Figs. 5 and 9). The shorelines in this area take a form of a flat gravel beach berm up to 30 m wide. On the surface they are composed of medium well-sorted gravel (clasts up to 4 cm) and little to no vegetation.

OSL sample LBSH1801 (850 m; Figs. 5 and 9) came from a road exposure of silty sediments that infill the valley bottom directly below the the 882 - 885 m asl shoreline. The sediments are laminated sandy silts with water escape features. Numerous boulders and cobbles are visible on the surface of the deposit but less frequently within the exposure. We interpret these sediments as glaciolacustrine sediments, which relate to the 882 - 885 shorelines.

The second OSL sample (RV1801, 893 m; Fig. 5) came from a horizontally - laminated silt and sand deposit situated inboard of the Rincon moraines in the Lacteo valley. We interpret this deposit as glaciolacustrine sediments from a smaller proglacial lake that formed in the Lacteo valley and was independent to the Belgrano palaeolake.

4.2. Chronology

4.2.1. Timing of the readvance

The Belgrano and Rincon moraines are contemporaneous and represent a readvance of the Belgrano and Lacteo glaciers. ^{10}Be ages from the outermost Belgrano moraine ridge range from 12.5 $\pm$ 0.4 ka to 13.6 $\pm$ 0.4 ka, and yield a weighted mean of 13.0 $\pm$ 0.5 ka. The innermost moraines yield ages ranging from 12.3 $\pm$ 0.4 ka to 13.8 $\pm$ 0.4 ka, with a weighted mean of 13.2 $\pm$ 0.6 ka (Table 3, Figs. 5 and 10). The ages from the inner and outer moraine ridges are statistically indistinguishable. Within the dating resolution, we cannot distinguish the individual advances, instead, we group the ages together to

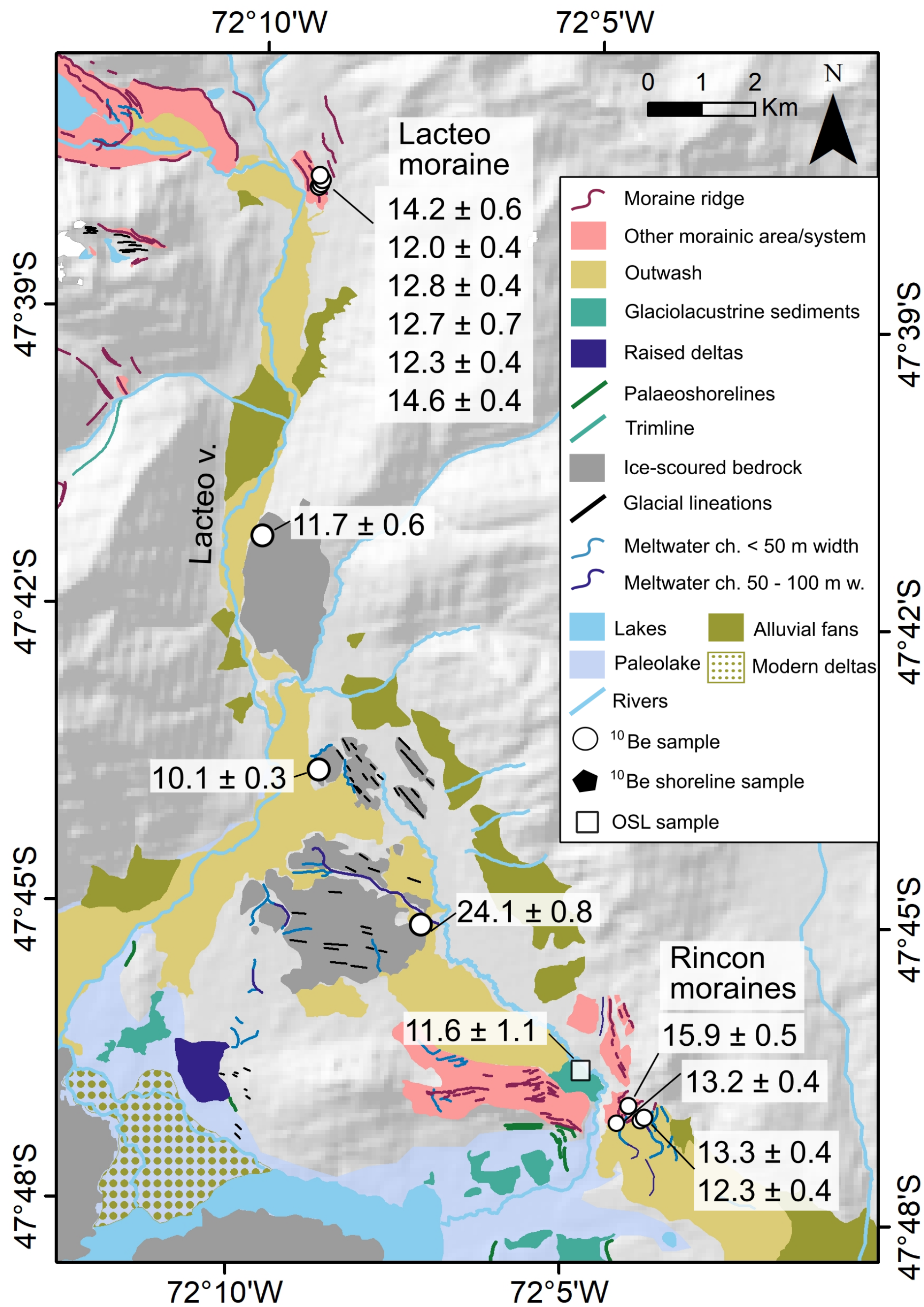

Figure 8: Enlarged geomorphology map of the Lacteo valley. Locations of samples collected from the Lacteo lateral moraine and along a transect in the valley are shown. The ^{10}Be ages presented here are individual ages with 1 σ internal uncertainty.

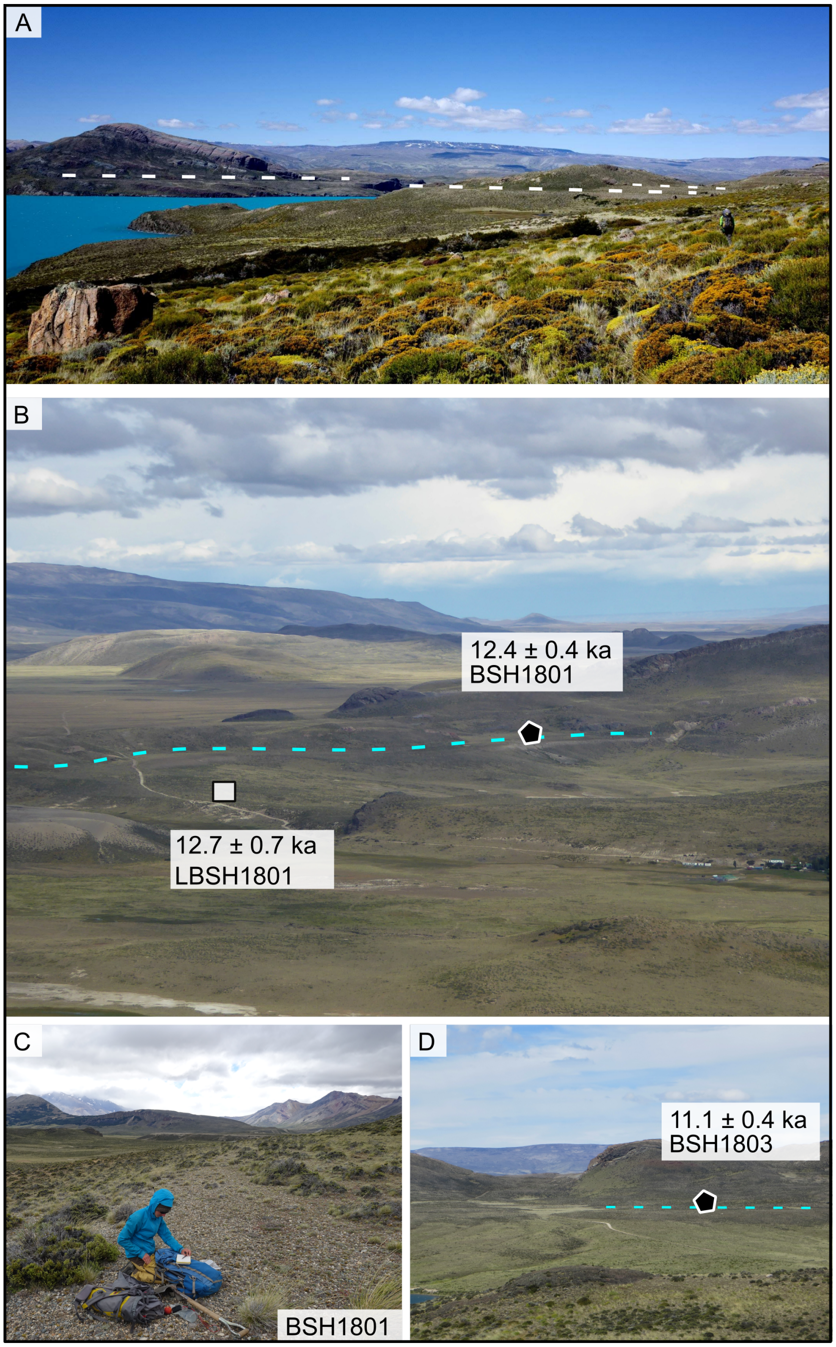

Figure 9: (A) Photograph showing raised shorelines above the modern Belgrano lake. (B) Photograph showing a palaeoshoreline with the location of surface exposure (black hexagon) and OSL (square) samples. The valley bottom below the shoreline is infilled with glaciolacutrine sediments. (C) Photograph showing the surface of a shoreline where sample BSH1801 was taken. (D) Photograph of a shoreline where sample BSH1803 was taken.

date the readvance at 13.1 ± 0.6 ka (weighted mean). The Rincon moraines yielded similar ages of 12.3 ± 0.4, 13.3 ± 0.4, and 13.2 ± 0.4 ka, and a weighted mean age of 12.9 ± 0.4 ka (Figs. 5 and 10 C). We excluded one sample with an older age of 15.9 ± 0.5 ka as an outlier.

4.2.2. Ice withdrawal and stabilisation

The Lacteo lateral moraine 20 km up valley from the Rincon moraines affords ages in range of 12.0 ± 0.4 ka to 14.6 ± 0.4 ka (Fig. 8). The ages display a significant spread and a bi-modal distribution (Fig. 10 D). All ages fall within 2 σ of the weighted mean of 13.0 ± 1.0 ka, and thus there is no statistical grounds for excluding any ages. However, the moraines are morphostratigraphically younger than the Rincon moraines (12.9 ± 0.4 ka), and so we exclude the older two ages (14.2 ± 0.6 and 14.6 ± 0.4 ka) as outliers and instead use the weighted mean of the younger ages to date the advance at 12.4 ± 0.3 ka. This interpretation fits with the wider chronology throughout the valley. The two older samples were probably reworked from an earlier advance.

Samples from a transect along the Río Lacteo valley (Fig. 8) yielded ages of 24.1 ± 0.8 (RV1608), 10.1 ± 0.3 (RV1606), and 11.7 ± 0.6 ka (RV1609) (in the order of distance from the Rincon moraines). The oldest sample is chronostratigraphically an outlier and likely relates to the gLGM. The remaining two ages likely afford minimum ages for deglaciation of the Lacteo valley. The sample RV1609 came from a cobble on a bedrock outcrop about 30 m higher in elevation than the sample RV1606, which could explain its older age despite being 4.5 km further up the valley.

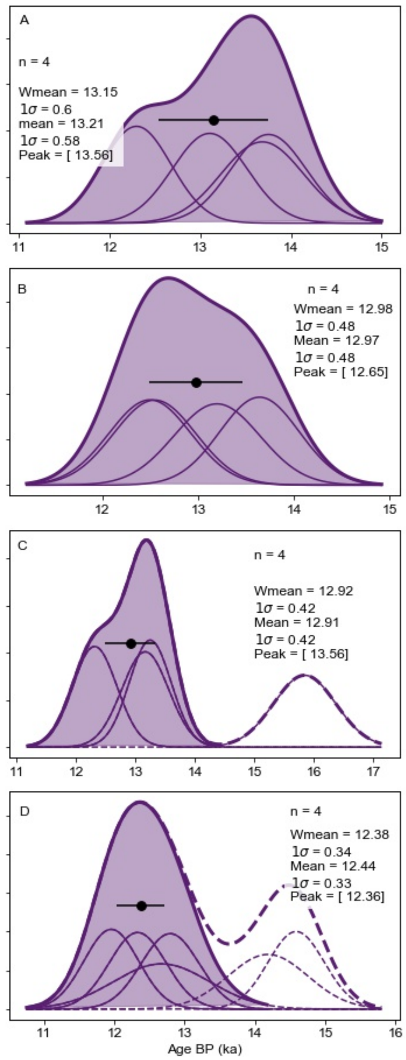

Figure 10: Normal kernel density diagrams for exposure ages from moraines: (A) the Belgrano inner moraines,(B) the Belgrano outer moraines, (C) the Rincon, and (D) the Lacteo lateral moraine. Thin purple curves represent Gaussian curves for each age and thick purple curves represent the summed probabilities. Outliers are represented by dashed lines. Circles represent uncertainties-weighted mean of ages after excluding the outliers, and 1 σ standard deviations.

4.2.3. Palaeolake development

The two ^{10}Be samples from the palaeo-shorelines yield ages of 12.4 ± 0.4 and 11.1 ± 0.4 ka, which is consistent with the slightly older ages for the Belgrano moraines (Table 3 and Fig. 5). The age difference between the two beach gravels could result from post-depositional processes or inheritance, and without additional samples it is difficult to resolve. The OSL sample (12.7 ± 0.7 ka) that came from glaciolacustrine sediments associated with the 882 - 885 shoreline is within dating uncertainties consistent with the shoreline ^{10}Be ages. The palaeolake likely formed at or before 12.7 ka and persisted for at least several hundred years, but perhaps over a millennium. The OSL sample from lacustrine sediments inboard of the Rincon moraines (Fig. 5), with an age of 11.6 ± 1.1 ka, fits with the slightly older ^{10}Be ages from the bounding Rincon moraines. This proglacial formed between the Lacteo glacier and the Rincon moraines, and likely drained into palaeolake Belgrano.

5. Discussion

5.1. LGIT at Lago Belgrano

Our ^{10}Be chronology indicates that a major re-advance of the Belgrano and Lacteo glaciers culminated at $\sim$ 13 ka toward the end of the ACR. At this time, the Belgrano glacier advanced to within 8 km of its gLGM limit (24.7 ± 1.0 ka, Mendelova et al., 2019). Our mapping reveals up to 10 advances/still-stands during the ACR, but the dating resolution is insufficient to distinguish between them. The reconstructed extent of the Belgrano and Lacteo glaciers during the ACR is shown in Figure 11.

Following the culmination of these advances/still-stands, the ice margin retreated and abandoned the Belgrano moraines. In the process, a palaeolake formed at 882 - 885 m asl, which was dammed by ice at least 10 km west of the Belgrano moraines. The OSL age (12.7 ± 0.7 ka) from glaciolacustrine sediments and the ^{10}Be ages from lake shorelines (12.4 ± 0.4 and 11.1 ± 0.4 ka) suggest that this lake formed at ~12.7 ka and likely existed throughout the YD period. A minimum radiocarbon age of 12.6 ± 0.06 cal ka BP (Wenzens, 2005; Fig. 2) for ice retreat from the Belgrano moraines is consistent with this interpretation. Based on the above ages and the extent of mapped shorelines, we infer a retreat of at least 10 km within several hundred years, which was probably facilitated by calving in the proglacial lake. Although glacial retreat had initiated, the ice remained extensive enough to maintain an ice dam capable of blocking the southward drainage route through Lago Nansen.

The extent of mapped shorelines suggests that by this time, the Lacteo glacier had separated from the Belgrano glacier, and retreated at least 5 km from the Rincon moraines (Fig. 11). A proglacial lake formed inboard of the Rincon moraines. The OSL age from the glaciolacustrine sediments here (11.6 ± 1.1 ka) suggest that this lake existed at roughly the same time as the paleaolake Belgrano. The lateral moraines further up the Lacteo valley, with an age of 12.4 ± 0.3 ka, indicates the glacier margin then stabilised during the YD. Two ages from bedrock outcrops in the Lacteo valley (10.1 ± 0.3 and 11.7 ± 0.6 ka) indicate that the lower part of the valley deglaciated by the end of YD.

The moraines bounding Lago Burmeister occupy the same morphostratigraphic position as the Belgrano moraines, suggesting that they represent an ACR advance of the Burmeister glacier. A minimum radiocarbon age from a kettle within these moraines (Wenzens, 2005), however suggests that they are mid-Holocene in age. Further chronological control would be needed to confirm this.

5.2. Deglaciation of the central sector of the PIS

The PIS had retreated and thinned significantly during the first phase of deglaciation after 18-19 ka (Boex et al., 2013; Hein et al., 2010; Henríquez et al., 2017), and had started to separate into the Northern Patagonian Icefield and the San Lorenzo ice cap by $\sim$ 15 ka (Davies et al., 2018; Thorndycraft et al., 2019). The major basins of Lago Puyerredón and Lago Buenos Aires had deglaciated by about 16 ka (Hein et al., 2010; Turner et al., 2005; Bendle et al., 2017; Boex et al., 2013). By the time of the ACR, ice margins of the Northern Patagonian Icefield were within a few tens of km of the modern glacier margins (75-100 km upstream of the LGM limits; Davies et al., 2018; Thorndycraft et al., 2019; Nimick et al., 2016). Northern and western outlet glaciers of the San Lorenzo ice cap were no longer interacting with the PIS, as evidenced by the ACR moraines deposited by the Tranquilo and Calluqueo glaciers (Davies et al., 2018; Sagredo et al., 2018).

Our chronology from the Belgrano valley provides robust evidence for glacier expansion in central Patagonia during the ACR. Cross-cutting of the older Menelik moraines by the ACR Belgrano moraines demonstrates that this was a re-advance, in the case of the Belgrano glacier, rather than a still-stand during overall deglaciation. Together with the data from the Salto and Tranquilo valleys (Davies et al., 2018; Sagredo et al., 2018), this indicates

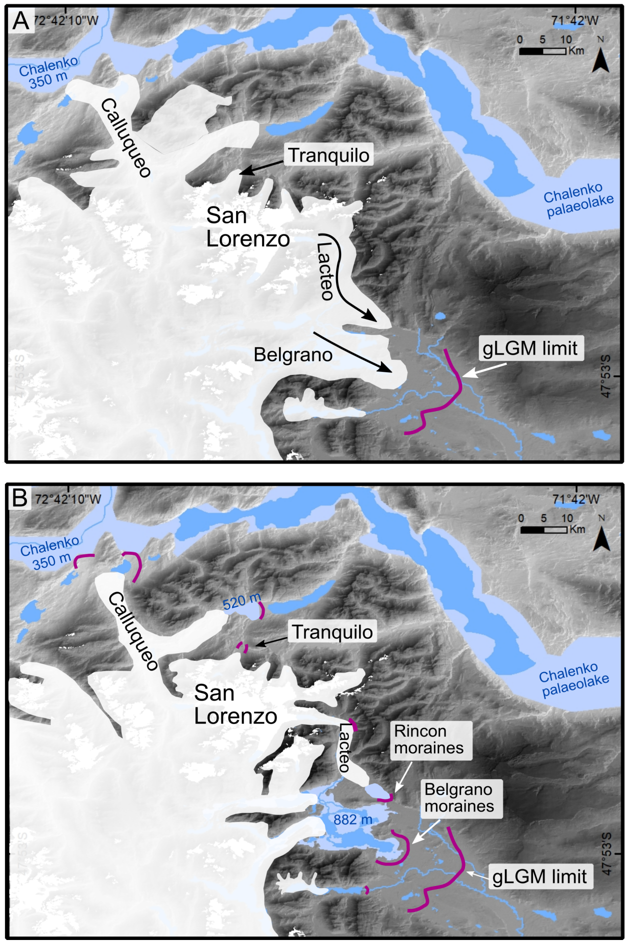

Figure 11: Model of ice and palaeolake evolution (A) during the ACR and (B) during the YD. The extent of the Belgrano and Lacteo glaciers during the ACR, and the extent of the palaeolake Belgrano during the YD are based on our geomorphological mapping and chronology. The extent of the Calluqueo and Tranquilo glaciers, and palaeolakes (pale blue) on the northern flanks of the San Lorenzo is based on published work (Davies et al., 2018; Sagredo et al., 2018; Glasser et al., 2012; Martin et al., 2019; Thorndycraft et al., 2019). Moraines delineating the extent of these glaciers are highlighted in pink. Elevation of the palaeolakes is also indicated in m asl. Darker blue colour indicates modern lakes.

a uniform response of the San Lorenzo glaciers to the ACR climate signal. To maintain an outlet glacier in the Belgrano valley, the ice cap likely also covered mountains to the south of the San Lorenzo massif, but the wider geomorphology suggest it was largely independent of the shrinking ice-sheet by this time.

Glacier advances/still-stands in central Patagonia during the ACR were a response to colder and wetter conditions reconstructed from pollen data. The Lago Edita record (47° S, Henríquez et al., 2017) revealed an increase in cold-resistant taxa between 14 ka - 13.5 ka. A northward expansion of the Magellanic moorland between 14.5 - 12.8 ka was documented by a marine pollen record off the Chilean coast (46° S, Montade et al., 2013; Fig. 12). These palaeovegetation changes were interpreted to indicate increased precipitation due to enhanced influence of the SWW at this latitude, and a pause in deglacial warming in the area (Henríquez et al., 2017; Montade et al., 2013).

Following the ACR advances, ice in the Belgrano valley retreated by at least 10 km before stabilising again. This is evidenced by the palaeolake Belgrano, which formed once ice abandoned the Belgrano moraines and existed during the YD period, as well as by the lateral moraines in the Lacteo valley (12.4 $\pm$ 0.3 ka). The initial ice recession was likely a response to regional warming trend as indicated by the retreat of the Magellanic moorland after 12.8 ka (Montade et al., 2013; Fig. 12), and palaeovegetation changes in the Lago Edita record (Henríquez et al., 2017). The YD ice margin stabilisation in central Patagonia is supported by provisional ^{10}Be ages from moraines inboard of the ACR limits in the Tranquilo and Salto valleys (Fig. 2; Glasser et al., 2012; Sagredo et al., 2018), and by ^{10}Be ages from the eastern side of the Northern Patagonian Icefield (Nimick et al., 2016; Glasser et al., 2012). Minor advances or still stands during the YD may reflect the continued influence of the SWW in central Patagonia. Pollen assemblages from the Lago Augusta core (47° S) were interpreted to indicate a highly variable precipitation regime under cool/wet climate between 13.8 and 11.8 ka (Villa-Martínez et al., 2012), while palaeovegetation changes in the Lago Edita record were interpreted to reflect the declining but continued influence of the SWW under warmer conditions until 11 ka (Henríquez et al., 2017).

Our data provide support for the final break-up and a complete separation of the PIS into the Northern Patagonian Icefield, the San Lorenzo and the Southern Patagonian Icefield by the end of the YD, when the ice-dammed palaeolake Belgrano drained. Our exposure ages from the palaeoshorelines (12.4 $\pm$ 0.4, 11.1 $\pm$ 0.4 ka) indicate that the Belgrano palaeolake likely drained at similar time as the palaeolake Chalenko (Fig. 11 with a Bayesian modelled age of 12 - 11 ka (Thorndycraft et al., 2019). By this time ice masses in central Patagonia were likely close to their present day configuration.

5.3. Factors controlling the relative magnitude of glacier advances

The ACR re-advance of the Belgrano glacier reached to within 8 km of its gLGM extent. This is in contrast with the ACR ice margins east of the Northern Patagonian Icefield and on the northern flank of San Lorenzo, which are $\sim$ 100 - 120 km upvalley from the gLGM limits. While the Belgrano ACR advance was primarily climatically controlled, the relative magnitude of the ACR and gLGM advances at Lago Belgrano can, at least in part, be explained by ice divide migration, catchment size and ice flow re-routing.

During the gLGM, the ice divide of the PIS was located west of San Lorenzo, along the main chain of the Andes. This potentially reduced the catchment size of the Belgrano glacier due to ice flow re-routing, while ice from the northern side of San Lorenzo was confluent with ice from the Northern Patagonian icefield and focused ice flow into the Lago Pueyrredón valley. This allowed a glacier in the Lago Pueyrredón valley to advance further east, while the Belgrano glacier was relatively small at the gLGM. The full elevation of the PIS also blocked westerly moisture penetration (Mendelova et al., 2019) and reduced snow fall over San Lorenzo during the gLGM further restricting the Belgrano glacier.

During deglaciation, the ice divide would have migrated eastward as the PIS thinned and broke down along its major basins, leading to ice flow reorganization and eventual ice divide break-up prior to the ACR. Glacier in the Lago Pueyrredón valley would have largely disintegrated by this time leaving ice margins of the former tributaries 100 - 120 km upstream of the gLGM limit (Hein et al., 2010; Turner et al., 2005; Boex et al., 2013; Henríquez et al., 2017). The thinning PIS would have also allowed for increased penetration of westerly precipitation to the San Lorenzo massif, relative to the gLGM, and enabled the Belgrano glacier to advance close to its gLGM limit. This process also explains why the Belgrano glacier was considerably smaller during the gLGM compared to its maximum extent of the last glacial cycle at ~ 75 ka (Mendelova et al., 2019). Thus, the real anomaly in the Belgrano valley is the comparatively small gLGM ice extent, rather than an exceptionally large ACR.

The catchment size and hypsometry also played a role in determining relative extents of the San Lorenzo glaciers during the ACR. The small extent of the Tranquilo glacier during the ACR, compared to the Belgrano and Calluqueo glaciers can be explained by their catchment size. While the former had a single smaller accumulation area on San Lorenzo (Sagredo et al., 2018), the latter two had additional ice contribution from the surrounding mountains. The difference in hypsometry will have played a role. The northern and western flanks of San Lorenzo have greater relief and a steeper elevation profile, and thus glaciers here would reach the ablation zone in a shorter distance when compared to ice discharging into the high elevation Belgrano valley to the east. A somewhat lower ELA on the western side of San Lorenzo (Falaschi et al., 2013), would have, to some extent, compensated for the lower altitude of the Salto valley and thereby allow the Calluqueo glacier to advance to the lower elevation of ~300 m asl Davies et al., 2018).

5.4. Regional view

Our data reveals a structure of the LGIT advances/still-stands at Lago Belgrano that is similar to southern Patagonia (51° S - 50° S; García et al., 2012; Moreno et al., 2009; Fogwill and Kubik, 2005; Ackert et al., 2008; Strelin et al., 2011; Kaplan et al., 2011) and New Zealand (Putnam et al., 2010a; Kaplan et al., 2010, 2013). Glaciers were most extensive during the ACR and then underwent recession punctuated by smaller advances/still-stands during the YD.

The ACR cooling is recorded in pollen records from NW Patagonia (41° - 43° S; Moreno and Videla, 2016; Pesce and Moreno, 2014), and a pause in deglacial warming coeval with the ACR is reflected in sea surface temperature records along the Chilean coast as far north as 41° S (Fig. 12; Kaiser et al., 2005; Haddam et al., 2018; Caniupán et al., 2011). At the moment, there are no glacial chronologies spanning the LGIT in northern Patagonia to evaluate the glacier response to cold reversals here. In southernmost Patagonia (54° S - 55° S), contradictory interpretations of the ACR extent of the Cordillera Darwin ice field warrant further work (McCulloch et al., 2005; Hall et al., 2013, 2017). East of the Cordillera Darwin, glaciers were confined to cirques during the ACR (Menounos et al., 2013). Colder climatic conditions during the ACR in Tierra del Fuego (53° S) are, however, indicated by palaeovegetation proxies (Mansilla et al., 2016).

Our data supports a widespread atmospheric and oceanic cooling throughout the southern mid-latitudes contemporaneous with cooling identified in the Antarctic ice cores (Fig. 12). Latitudinal displacement of the SWW belt and associated oceanic fronts could facilitate the propagation of the climate signals (Pesce and Moreno, 2014; Moreno et al., 2012; Lamy, 2004). A northward shift of the coupled system during the ACR would have caused cooling and increased precipitation, promoting glacier expansion in Patagonia and New Zealand (García et al., 2012; Sagredo et al., 2018; Putnam et al., 2010b). Such a shift in the coupled system was likely driven by interhemispheric oceanic teleconnections and associated atmospheric reorganization commonly attributed to the bipolar see-saw (Pedro et al., 2018; Stocker and Johnsen, 2003; Buizert et al., 2018).

6. Conclusions

Our geomorphological mapping along with ^{10}Be and OSL ages document a major re-advance of the Belgrano glacier at 13.1 ± 0.6 ka, and a

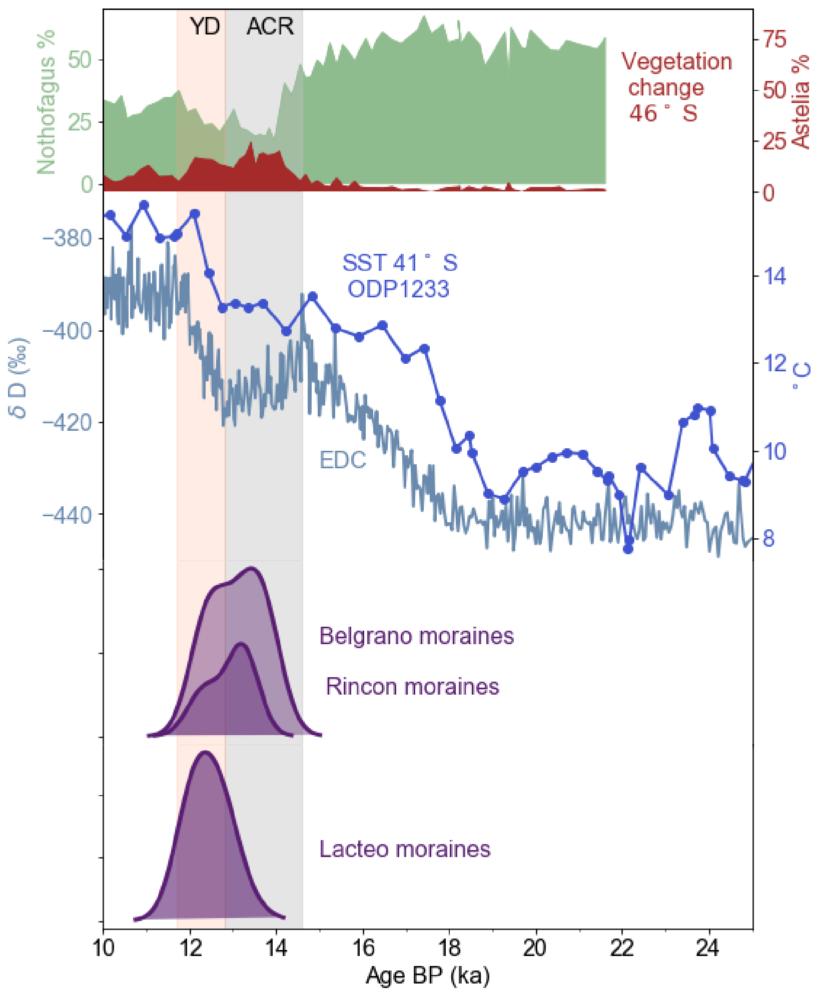

Figure 12: Comparison of our exposure ages to other proxies: *Nothofagus dombeyi* type and *Astelia pumila* pollen record from core MD07-3088 off the Chilean coast (46° S, Montade et al., 2013) plotted on on a scale from Montade et al. (2019), sea surface temperature reconstruction from core ODP 1233 off the Chilean coast (Kaiser et al., 2005) and the δ D record from EDC, east Antarctica (EPICA Community Members, 2004) plotted on AICC2012 timescale (Veres et al., 2013). The exposure ages are plotted after outliers have been removed. *Astelia* is a plant typical of the Magellanic moorland that at present grows south of 48° S.

re-advance/still-stand of the Lacteo glacier at 12.9 $\pm$ 0.4 ka, coeval with the ACR. The San Lorenzo ice cap covered an extensive area at this time, but was largely independent of at least the Northern Patagonian Icefield. Following the culmination of the ACR advances/still-stands, ice in the Belgrano valley retreated by at least 10 km and an ice-dammed proglacial lake formed at 882 - 885 m asl. The ^{10}Be ages from the palaeoshorelines and an OSL age from glaciolacustrine sediments suggest that the lake likely existed between $\sim$12.7 and $\sim$11.1 ka, implying stabilisation of ice margins during the YD. The ^{10}Be ages from a lateral moraine in the Lacteo valley (12.4 $\pm$ 0.3 ka) indicate a smaller advance/still-stand during the YD. We suggest that the final break-up of the PIS occurred at the end of the YD, when glaciers retreated back to the mountains and the palaeolake Belgrano drained. Our data from the Belgrano valley supports the dominant ACR climate signal in the southern mid-latitudes, but also suggest a co-occurrence of the northern hemisphere YD signal, albeit of smaller magnitude. Glacier expansion in the southern mid-latitudes during the ACR is in line with the northward migration of the coupled oceanic-atmospheric system.

Acknowledgements

This work was supported by a NERC PhD studentship (NE/L002558/1) to MM and a NERC CIAF grant (CIAF.9167.0416). We also acknowledge funding from the British Society for Geomorphology, Quaternary Research Association, Royal Geographical Society (with IBG), the Explorers Club, the Scottish Alliance for Geoscience, Environment and Society (Small Grants Scheme), and the Moray Endowment Fund from the University of Edinburgh.

We are grateful to Andrew Gray for his help with fieldwork and Patricio Parada for arranging export of samples. The national park authorities of Argentina are thanked for granting permission to conduct fieldwork, and the rangers of the Perito Moreno National Park are thanked in particular for their assistance in the field. Jenny Bradley is thanked for preparing the samples for OSL dating at the University of Liverpool. We would like to thank D.Sugden and R.McCulloch for insightful discussions. Bethan Davies and Mike Bentley are thanked for their constructive comments that greatly improved this manuscript.

Supplementary Information

OSL methods

Samples for luminescence dating were collected in opaque tubes and prepared for analysis under subdued lighting conditions. To calculate the environmental dose-rate throughout burial for each sample, U, Th and K concentrations were measured for $\sim$ 80 g of the bulk sediment sample using high-resolution gamma spectrometry. Water contents of 5 $\pm$ 2 % were estimated considering the field water contents, and the environmental history for each sample. Cosmic dose-rates were calculated after Prescott and Hutton (1994). Environmental dose-rates determined for samples RV1801 and LBSH1801 are shown in Table S1. Grains of K-feldspar were used to determine equivalent doses (D_e). Samples were first treated with a 10 % v/v dilution of 37 % HCl and with 20 % v/v of H_2O_2 to remove carbonates and organics, respectively. Dry sieving then isolated the 125 - 180 μm (sample LBSH1801) or 212 - 250 μm (sample RV1801) diameter grains, which were subject to density separation using sodium polytungstate (< 2.58 g cm^{-3} K-feldspar dominated) and then not etched using hydrofluoric acid. Finally, grains of K-feldspar were mounted on a 9.8 mm diameter aluminium single-grain disc for analysis, which contained a 10 by 10 grid of 300 μm diameter holes. Note that sample LBSH01-01 was analysed using microhole analysis rather than single grains (i.e. up to four grains in each hole due to a grain size of 125 - 180 μm). All luminescence measurements were performed using a RisøTL/OSL DA-15 automated single-grain system equipped with a ^{90}Sr/^{90}Y beta source (Bøtter-Jensen et al., 2003) fitted with a blue filter pack (BG39, Coring 7-59) in front of the photomultiplier tube. Single aliquot regenerative dose (SAR) protocols (Murray and Wintle, 2000) were used for the post-IR IRSL analyses performed at 225 $°C$ (Thomsen et al., 2008), termed the pIRIR$_{225}$ signal. A preheat temperature of 250 $°C$ for 60 s was used prior to stimulations of 2 s using the infra-red laser at 225 $°C$. The IRSL signal measured performed at 50 $°C$ prior to the pIRIR$_{225}$ measurement and the elevated temperature bleach of 330 $°C$ for 200 s at the end of each L_x/T_x cycle were performed using the IR LEDs. The location of the single-grain discs was performed at room temperature, rather than elevated temperatures to prevent thermal annealing of the IRSL signal (after Smedley and Duller, 2013). The first 0.3 s and final 0.6 s of stimulation were summed to calculate the initial and background IRSL signals, respectively. The grains were accepted after applying the following screening criteria and accounting for the associated uncertainties: (1) whether the test dose response was greater than three sigma above the background, (2) whether the test dose uncertainty was less than 10 %, (3) whether the recycling and OSL-IR depletion ratios were within the range of ratios 0.9 to 1.1, and (4) whether recuperation was less than 5 % of the response from the largest regenerative dose. Grains from both samples were used for dose-recovery experiments and successfully recovered a given dose within 10 % using the $pIRIR_{225}$ signal. Fading experiments were performed on three multi-grain aliquots per sample and reported g-values of -0.4 $\pm$ 0.7 %/decade (RV18-01) and -1.0 $\pm$ 0.7 %/decade (LBSH18-01), which suggests that no fading correction was required for the $pIRIR_{225}$ signal. D_e values were calculated from all grains passing all the screening criteria. The minimum age model (MAM; (Galbraith et al., 1999; Galbraith and Laslett, 1993)) was applied to determine an age for the samples as the asymmetrical D_e distributions suggested the samples were partially bleached prior to burial (Fig. S1). The scatter in the D_e distribution arising from intrinsic and extrinsic sources were combined in quadrature to determine σb for the MAM (Table S1). The overdispersion values arising from intrinsic sources for sample RV1801 (12 %) and LBSH18-01 (13 %) were derived from the dose-recovery experiments, while the over-dispersion arising from variability in the internal dose-rates of K-feldspar grains for both samples was assumed to be 10 % (after Smedley and Pearce, 2016). Additional over-dispersion (20 %) was incorporated for sample RV1801 to account for the variability in single-grain D_e distributions caused by external microdosimetry (after Smedley et al. 2017). The D_e values were then divided by the environmental dose-rates to determine an age for each sample (Table S1).

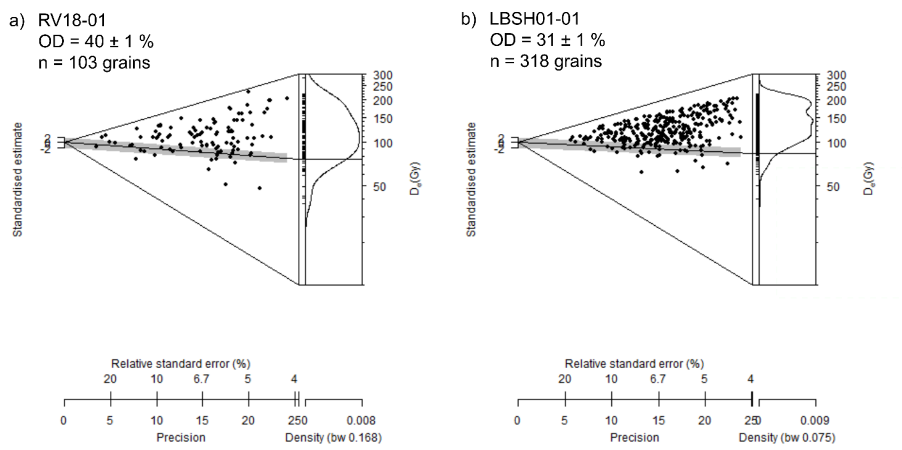

Figure 1: Abanico plots of the D_e values determined for OSL dating, where the grey shading shows the MAM D_e for each distribution. Note that sample LBSH0101 was analysed using microhole analysis rather than single grains (i.e. up to four grains in each hole due to a grain size of 125 180 μm) but it is likely that the OSL signal was dominated by one brighter grain.

References

Ackert, R., Becker, R.A., Singer, B.S., Kurz, M.D., Caffee, M.W., Mickelson, D.M., 2008. Patgonian Glacier Response during the Late Glacial Holocene Transition. Science 321, 392–396.

Anderson, R.F., Ali, S., Bradtmiller, L.I., Nielsen, S.H.H., Fleisher, M.Q., Anderson, B.E., Burckle, L.H., 2009. Wind-Driven Upwelling in the Southern Ocean and the Deglacial Rise in Atmospheric CO2. Science 323, 1443–1448.

Balco, G., Stone, J.O., Lifton, N.A., Dunai, T.J., 2008. A complete and easily accessible means of calculating surface exposure ages or erosion rates from 10Be and 26Al measurements. Quaternary Geochronology 3, 174–195.

Bendle, J.M., Thorndycraft, V.R., Palmer, A.P., 2017. The glacial geomorphology of the Lago Buenos Aires and Lago Pueyrredón ice lobes of central Patagonia. Journal of Maps 13, 654–673.

Bennett, K.D., 2000. The Last Glacial-Holocene Transition in Southern Chile. Science 290, 325–328.

Björck, S., Rundgren, M., Ljung, K., Unkel, I., Wallin, ., 2012. Multi-proxy analyses of a peat bog on Isla de los Estados, easternmost Tierra del Fuego: A unique record of the variable Southern Hemisphere Westerlies since the last deglaciation. Quaternary Science Reviews 42, 1–14.

Blunier, T., Chappellaz, J., Schwander, J., Dällenbach, A., Stauffer, B., Stocker, T.F., Raynaud, D., Jouzel, J., Clausen, H.B., Hammer, C.U., Johnsen, S.J., 1998. Asynchrony of Antarctic and Greenland climate change during the last glacial period. Nature 394, 739–743.

Boex, J., Fogwill, C., Harrison, S., Glasser, N.F., Hein, A., Schnabel, C., Xu, S., 2013. Rapid thinning of the late Pleistocene Patagonian Ice Sheet followed migration of the Southern Westerlies. Scientific Reports 3, 2118.

Borchers, B., Marrero, S., Balco, G., Caffee, M., Goehring, B., Lifton, N., Nishiizumi, K., Phillips, F., Schaefer, J., Stone, J., 2016. Geological calibration of spallation production rates in the CRONUS-Earth project. Quaternary Geochronology 31, 188–198.

Bøtter-Jensen, L., Andersen, C., Duller, G., Murray, A., 2003. Developments in radiation, stimulation and observation facilities in luminescence measurements. Radiation Measurements 37, 535–541.

Bronk Ramsey, C., 2009. Bayesian Analysis of Radiocarbon Dates. Radiocarbon 51, 337–360.

Buizert, C., Sigl, M., Severi, M., Markle, B.R., Wettstein, J.J., McConnell, J.R., Pedro, J.B., Sodemann, H., Goto-Azuma, K., Kawamura, K., Fujita, S., Motoyama, H., Hirabayashi, M., Uemura, R., Stenni, B., Parrenin, F., He, F., Fudge, T.J., Steig, E.J., 2018. Abrupt ice-age shifts in southern westerly winds and Antarctic climate forced from the north. Nature 563, 681–685.

Caldenius, C., 1932. Las glaciaciones cuaternarias en la Patagonia y Tierra del Fuego. Geografiska Annaler 14, 1–164.

Caniupán, M., Lamy, F., Lange, C.B., Kaiser, J., Arz, H., Kilian, R., Baeza Urrea, O., Aracena, C., Hebbeln, D., Kissel, C., Laj, C., Mollenhauer, G., Tiedemann, R., 2011. Millennial-scale sea surface temperature and Patagonian Ice Sheet changes off southernmost Chile (53 °S) over the past 60 kyr. Paleoceanography 26, 1–10.

Darvill, C.M., 2013. Cosmogenic nuclide analysis. Geomophological techniques 10, 1–25.

Darvill, C.M., Stokes, C.R., Bentley, M.J., Lovell, H., 2014. A glacial geomorphological map of the southernmost ice lobes of Patagonia: the Bahía Inútil San Sebastián, Magellan, Otway, Skyring and Río Gallegos lobes. Journal of Maps 10, 500–520.

Davies, B., Thorndycraft, V., Fabel, D., Martin, J., 2018. Asynchronous glacier dynamics during the Antarctic Cold Reversal in central Patagonia. Quaternary Science Reviews 200, 287–312.

De Angelis, H., Miles, E., Moelg, N., Paul, F., Sharp, M., Wyatt, F., 2015. GLIMS Glacier Database.

De Arellano, C.R., Putlitz, B., Müntener, O., Ovtcharova, M., 2012. High precision U/Pb zircon dating of the Chaltén Plutonic Complex (Cerro Fitz Roy, Patagonia) and its relationship to arc migration in the southernmost Andes. Tectonics 31.

Denton, G., Heusser, C.J., Lowel, T., Moreno, P., Andersen, B., Heusser, L.E., Schluhter, C., Marchant, D., 1999. Interhemispheric Linkage of Paleoclimate During the Last Glaciation. Geografiska Annaler, Series A: Physical Geography 81, 107–153.

Denton, G.H., Anderson, R.F., Toggweiler, J.R., Edwards, R.L., Schaefer, J.M., Putnam, a.E., 2010. The Last Glacial Termination. Science 328, 1652–1656.

Douglass, D.C., Singer, B.S., Ackert, R.P., Kaplan, M.R., Caffee, M.W., 2007. Constraining Boulder Erosion Rates and Ages of Mid-Pleistocene Moraines. Lago Buenos Aires, Argentina. GSA Abstracts and Programs Northeastern Section, 42nd Annual Meeting .

EPICA Community Members, 2004. Eight glacial cycles from an Antarctic ice core. Nature 429, 623–628.

Falaschi, D., Bolch, T., Rastner, P., Lenzano, M.G., Lenzano, L., Lo Vecchio, A., Moragues, S., 2017. Mass changes of alpine glaciers at the eastern margin of the Northern and Southern Patagonian Icefields between 2000 and 2012. Journal of Glaciology 63, 258–272.

Falaschi, D., Bravo, C., Masiokas, M., Villalba, R., Rivera, A., 2013. First Glacier Inventory and Recent Changes in Glacier Area in the Monte San Lorenzo Region (47°S), Southern Patagonian Andes, South America. Arctic, Antarctic, and Alpine Research 45, 19–28.

Fogwill, C.J., Kubik, P.W., 2005. A glacial stage spanning the Antarctic Cold Reversal in Torres del Paine (51°S), Chile, based on preliminary cosmogenic exposure ages. Geografiska Annaler, Series A: Physical Geography 87, 403–408.

Galbraith, R., Laslett, G., 1993. Statistical models for mixed fission track ages. Nuclear Tracks and Radiation Measurements 21, 459–470.

Galbraith, R.F., Roberts, R.G., Laslett, G.M., Yoshida, H., Olley, J.M., 1999. Optical dating of single and multiple grains of quartz from Jinmium rock shelter, northern Australia: Part I, experimental design and statistical models. Archaeometry 41, 339–364.

García, J.L., Kaplan, M.R., Hall, B.L., Schaefer, J.M., Vega, R.M., Schwartz, R., Finkel, R., 2012. Glacier expansion in southern Patagonia throughout the Antarctic cold reversal. Geology 40, 859–862.

Garibotti, I.A., Villalba, R., 2017. Colonization of mid- and late-Holocene moraines by lichens and trees in the Magellanic sub-Antarctic province. Polar Biology 40, 1739–1753.

Garreaud, R., Lopez, P., Minvielle, M., Rojas, M., 2013. Large-scale control on the Patagonian climate. Journal of Climate 26, 215–230.

Glasser, N.F., Harrison, S., Schnabel, C., Fabel, D., Jansson, K.N., 2012. Younger Dryas and early Holocene age glacier advances in Patagonia. Quaternary Science Reviews 58, 7–17.

Glasser, N.F., Jansson, K.N., Harrison, S., Kleman, J., 2008. The glacial geomorphology and Pleistocene history of South America between 38°S and 56°S. Quaternary Science Reviews 27, 365–390.

Glasser, N.F., Jansson, K.N., Harrison, S., Rivera, A., 2005. Geomorphological evidence for variations of the North Patagonian Icefield during the Holocene. Geomorphology 71, 263–277.

Gosse, J.C., Phillips, F.M., 2001. Terrestrial in situ cosmogenic nuclides: Theory and application. Quaternary Science Reviews 20, 1475–1560.

Haberle, S.G., Bennett, K.D., 2004. Postglacial formation and dynamics of North Patagonian Rainforest in the Chonos Archipelago, Southern Chile. Quaternary Science Reviews 23, 2433–2452.

Haddam, N.A., Siani, G., Michel, E., Kaiser, J., Lamy, F., Duchamp-Alphonse, S., Hefter, J., Braconnot, P., Dewilde, F., Isgüder, G., Tisnerat-Laborde, N., Thil, F., Durand, N., Kissel, C., 2018. Changes in latitudinal sea surface temperature gradients along the Southern Chilean margin since the last glacial. Quaternary Science Reviews 194, 62–76.

Hall, B.L., Denton, G., Lowell, T., Bromley, G.R.M., Putnam, A.E., 2017. Retreat of the Cordillera Darwin icefield during Termination I. Cuadernos de Investigación Geográfica 0.

Hall, B.L., Porter, C.T., Denton, G.H., Lowell, T.V., Bromley, G.R.M., 2013. Extensive recession of Cordillera Darwin glaciers in southernmost South America during Heinrich Stadial 1. Quaternary Science Reviews 62, 49–55.

Hein, A.S., Cogez, A., Darvill, C.M., Mendelova, M., Kaplan, M.R., Herman, F., Dunai, T.J., Norton, K., Xu, S., Christl, M., Rodés, ., 2017. Regional mid-Pleistocene glaciation in central Patagonia. Quaternary Science Reviews 164, 77–94.

Hein, A.S., Hulton, N.R., Dunai, T.J., Sugden, D.E., Kaplan, M.R., Xu, S., 2010. The chronology of the Last Glacial Maximum and deglacial events in central Argentine Patagonia. Quaternary Science Reviews 29, 1212–1227.

Henríquez, W.I., Villa-Martínez, R., Vilanova, I., De Pol-Holz, R., Moreno, P.I., 2017. The last glacial termination on the eastern flank of the central Patagonian Andes (47 ° S). Climate of the Past 13, 879–895.

Hogg, A.G., Hua, Q., Blackwell, P.G., Niu, M., Buck, C.E., Guilderson, T.P., Heaton, T.J., Palmer, J.G., Reimer, P.J., Reimer, R.W., Turney, C.S.M., Zimmerman, S.R.H., 2013. SHCal13 Southern Hemisphere Calibration, 050,000 Years cal BP. Radiocarbon 55, 1889–1903.

Horta, L.R., Georgieff, S.M., Aschero, C.A., Goñi, R.A., 2017. Paleolacustrine records from Late Pleistocene Holocene in the Perito Moreno National Park, Argentinian Patagonian Andes. Quaternary International 436, 8–15.

Iglesias, V., Markgraf, V., Whitlock, C., 2016. 17,000 years of vegetation, fire and climate change in the eastern foothills of the Andes (lat. 44°S). Palaeogeography, Palaeoclimatology, Palaeoecology 457, 195–208.

Kaiser, J., Lamy, F., Hebbeln, D., 2005. A 70-kyr sea surface temperature record off southern Chile (Ocean Drilling Program Site 1233). Paleoceanography 20, PA4009.

Kaplan, M.R., Schaefer, J.M., Denton, G.H., Barrell, D.J.A., Chinn, T.J.H., Putnam, A.E., Andersen, B.G., Finkel, R.C., Schwartz, R., Doughty, A.M., 2010. Glacier retreat in New Zealand during the Younger Dryas stadial. Nature 467, 194–197.

Kaplan, M.R., Schaefer, J.M., Denton, G.H., Doughty, A.M., Barrell, D.J.A., Chinn, T.J.H., Putnam, A.E., Andersen, B.G., Mackintosh, A., Finkel, R.C., Schwartz, R., Anderson, B., 2013. The anatomy of long-term warming since 15 ka in New Zealand based on net glacier snowline rise. Geology 41, 887–890.

Kaplan, M.R., Strelin, J.A., Schaefer, J.M., Denton, G.H., Finkel, R.C., Schwartz, R., Putnam, A.E., Vandergoes, M.J., Goehring, B.M., Travis, S.G., 2011. In-situ cosmogenic 10Be production rate at Lago Argentino, Patagonia: Implications for late-glacial climate chronology. Earth and Planetary Science Letters 309, 21–32.

Lal, D., 1991. Cosmic ray labeling of erosion surfaces: in situ nuclide production rates and erosion models. Earth and Planetary Science Letters 104, 424–439.

Lamy, F., 2004. Antarctic Timing of Surface Water Changes off Chile and Patagonian Ice Sheet Response. Science 304, 1959–1962.

Lamy, F., Kaiser, J., Arz, H.W., Hebbeln, D., Ninnemann, U., Timm, O., Timmermann, A., Toggweiler, J., 2007. Modulation of the bipolar seesaw in the Southeast Pacific during Termination 1. Earth and Planetary Science Letters 259, 400–413.

Lemieux-Dudon, B., Blayo, E., Petit, J.R., Waelbroeck, C., Svensson, A., Ritz, C., Barnola, J.M., Narcisi, B.M., Parrenin, F., 2010. Consistent dating for Antarctic and Greenland ice cores. Quaternary Science Reviews 29, 8–20.

Lumley, S., Switsur, R., 1993. Late Quaternary Chronology of the Taitao peninsula, southern Chile. Journal of Quaternary Science 8, 161–165.

Mansilla, C.A., McCulloch, R.D., Morello, F., 2016. Palaeoenvironmental change in Southern Patagonia during the Lateglacial and Holocene: Implications for forest refugia and climate reconstructions. Palaeogeography, Palaeoclimatology, Palaeoecology 447, 1–11.

Markgraf, V., Whitlock, C., Haberle, S., 2007. Vegetation and fire history during the last 18,000 cal yr B.P. in Southern Patagonia: Mallín Pollux, Coyhaique, Province Aisén (45°4130 S, 71°5030 W, 640 m elevation). Palaeogeography, Palaeoclimatology, Palaeoecology 254, 492–507.

Marshall, J., Speer, K., 2012. Closure of the meridional overturning circulation through Southern Ocean upwelling. Nature Geoscience 5, 171–180.

Martin, J.R., Davies, B.J., Thorndycraft, V.R., 2019. Glacier dynamics during a phase of Late Quaternary warming in Patagonia reconstructed from sediment-landform associations. Geomorphology 337, 111–133.

McCulloch, R., Bentley, M., Tipping, R., Clapperton, C., 2005. Evidence for LateGlacial Ice Dammed Lakes In The Central Strait Of Magellan And Bahía Inútil, Southernmost South America. Geografiska Annaler, Series A: Physical Geography 87, 335–362.

Meijers, A.J., 2014. The Southern Ocean in the Coupled Model Intercomparison Project phase 5. Philosophical Transactions of the Royal Society A: Mathematical, Physical and Engineering Sciences 372.

Mendelova, M., Hein, A., McCulloch, R., Davies, B., 2017. The Last Glacial Maximum and deglaciation in central Patagonia, 44°S49°S. Cuadernos de Investigación Geográfica 43, 719.

Mendelova, M., Hein, A.S., Rodes, A., Xu, S., 2019. Extensive mountain glaciation in central Patagonia during Marine Isotope Stage 5. Quaternary Science Reviews (Accepted).

Menounos, B., Clague, J.J., Osborn, G., Davis, P.T., Ponce, F., Goehring, B.M., Maurer, M., Rabassa, J.O., Coronato, A., Marr, R., 2013. Latest Pleistocene and Holocene glacier fluctuations in southernmost Tierra del Fuego, Argentina. Quaternary Science Reviews 77, 70–79.

Mercer, J.H., 1984. Simultaneous climatic change in both hemispheres and similar bipolar interglacial warming: Evidence and implications, in: Hansen, J.E., Takahashi, T. (Eds.), Climate Processes and Climate Sensitivity. American Geophysical Union, Washington, D. C.. volume 29 of *Geophysical Monograph Series*, pp. 307–313.

Montade, V., Combourieu Nebout, N., Kissel, C., Haberle, S.G., Siani, G., Michel, E., 2013. Vegetation and climate changes during the last 22,000yr from a marine core near Taitao Peninsula, southern Chile. Palaeogeography, Palaeoclimatology, Palaeoecology 369, 335–348.

Montade, V., Peyron, O., Favier, C., Francois, J.P., Haberle, S.G., 2019. A pollen-climate calibration from western Patagonia for palaeoclimatic reconstructions. Journal of Quaternary Science 34, 76–86.

Moreno, P.I., Kaplan, M.R., François, J.P., Villa-Martínez, R., Moy, C.M., Stern, C.R., Kubik, P.W., 2009. Renewed glacial activity during the Antarctic cold reversal and persistence of cold conditions until 11.5 ka in southwestern Patagonia. Geology 37, 375–378.

Moreno, P.I., Videla, J., 2016. Centennial and millennial-scale hydroclimate changes in northwestern Patagonia since 16,000 yr BP. Quaternary Science Reviews 149, 326–337.

Moreno, P.I., Villa-Martínez, R., Cárdenas, M.L., Sagredo, E.A., 2012. Deglacial changes of the southern margin of the southern westerly winds revealed by terrestrial records from SW Patagonia (52°S). Quaternary Science Reviews 41, 1–21.

Murdie, R.E., Pugh, D.T., Styles, P., 1998. A lightweight, portable, digital probe for measuring the thermal gradient in shallow water sediments, with examples from Patagonia. Geo-Marine Letters 18, 315–320.

Murray, A., Wintle, A., 2000. Luminescence dating of quartz using an improved single-aliquot regenerative-dose protocol. Radiation Measurements 32, 57–73.

Nimick, D.A., McGrath, D., Mahan, S.A., Friesen, B.A., Leidich, J., 2016. Latest Pleistocene and Holocene glacial events in the Colonia valley, Northern Patagonia Icefield, southern Chile. Journal of Quaternary Science 31, 551–564.

Pedro, J.B., Jochum, M., Buizert, C., He, F., Barker, S., Rasmussen, S.O., 2018. Beyond the bipolar seesaw: Toward a process understanding of interhemispheric coupling. Quaternary Science Reviews 192, 27–46.

Pesce, O.H., Moreno, P.I., 2014. Vegetation, fire and climate change in central-east Isla Grande de Chiloé (43°S) since the Last Glacial Maximum, northwestern Patagonia. Quaternary Science Reviews 90, 143–157.

de Porras, M.E., Maldonado, A., Abarzúa, A.M., Cárdenas, M.L., Francois, J.P., Martel-Cea, A., Stern, C.R., Méndez, C., Reyes, O., 2012. Postglacial vegetation, fire and climate dynamics at Central Chilean Patagonia (Lake Shaman, 44°S). Quaternary Science Reviews 50, 71–85.

de Porras, M.E., Maldonado, A., Quintana, F.A., Martel-Cea, A., Reyes, O., Méndez, C., 2014. Environmental and climatic changes in central Chilean Patagonia since the Late Glacial (Mallín El Embudo, 44°S). Climate of the Past 10, 1063–1078.

Putkonen, J., Swanson, T., 2003. Accuracy of cosmogenic ages for moraines. Quaternary Research 59, 255–261.

Putnam, A.E., Denton, G.H., Schaefer, J.M., Barrell, D.J.A., Andersen, B.G., Finkel, R.C., Schwartz, R., Doughty, A.M., Kaplan, M.R., Schlüchter, C., 2010a. Glacier advance in southern middle-latitudes during the Antarctic Cold Reversal. Nature Geoscience 3, 700–704.

Putnam, A.E., Schaefer, J.M., Barrell, D.J.A., Vandergoes, M., Denton, G.H., Kaplan, M.R., Finkel, R.C., Schwartz, R., Goehring, B.M., Kelley, S.E., 2010b. In situ cosmogenic 10Be production-rate calibration from the Southern Alps, New Zealand. Quaternary Geochronology 5, 392–409.

Ramos, V.A., Kay, S.M., 1992. Southern Patagonian plateau basalts and deformation: Backarc testimony of ridge collisions. Tectonophysics 205, 261–282.

Sagredo, E.A., Kaplan, M.R., Araya, P.S., Lowell, T.V., Aravena, J.C., Moreno, P.I., Kelly, M.A., Schaefer, J.M., 2018. Trans-pacific glacial response to the Antarctic Cold Reversal in the southern mid-latitudes. Quaternary Science Reviews 188, 160–166.

Smedley, R.K., Duller, G., 2013. Optimising the reproducibility of measurements of the post-IR IRSL signal from single-grains of K-feldspar for dating. Ancient TL 31, 49–58.

Smedley, R.K., Glasser, N.F., Duller, G.A.T., 2016. Luminescence dating of glacial advances at Lago Buenos Aires (˜46°S), Patagonia. Quaternary Science Reviews 134, 59–73.

Smedley, R.K., Pearce, N.J., 2016. Internal U, Th and Rb concentrations of alkali-feldspar grains: Implications for luminescence dating. Quaternary Geochronology 35, 16–25.

Stocker, T.F., Johnsen, S.J., 2003. A minimum thermodynamic model for the bipolar seesaw. Paleoceanography 18, 1–9.

Stone, J.O., 2000. Air pressure and cosmogenic isotope production. Journal of Geophysical Research: Solid Earth 105, 23753–23759.

Strelin, J.A., Denton, G.H., Vandergoes, M.J., Ninnemann, U.S., Putnam, A.E., 2011. Radiocarbon chronology of the late-glacial Puerto Bandera moraines, Southern Patagonian Icefield, Argentina. Quaternary Science Reviews 30, 2551–2569.

Sugden, D., Bentley, M., Fogwill, C., Hulton, N., Mcculloch, R., Purves, R., 2005. Lateglacial glacier events in southernmost south america: a blend of northern and 'southern hemispheric climatic signals? Geografiska Annaler: Series A, Physical Geography 87, 273–288.

Thomsen, K., Murray, A., Jain, M., Bøtter-Jensen, L., 2008. Laboratory fading rates of various luminescence signals from feldspar-rich sediment extracts. Radiation Measurements 43, 1474–1486.

Thorndycraft, V.R., Bendle, J.M., Benito, G., Davies, B.J., Sancho, C., Palmer, A.P., Fabel, D., Medialdea, A., Martin, J.R., 2019. Glacial lake evolution and Atlantic-Pacific drainage reversals during deglaciation of the Patagonian Ice Sheet. Quaternary Science Reviews 203, 102–127.

Toggweiler, J.R., Russell, J.L., Carson, S.R., 2006. Midlatitude westerlies, atmospheric CO2, and climate change during the ice ages. Paleoceanography 21, 1–15.

Turner, K.J., Fogwill, C.J., McCulloch, R.D., Sugden, D.E., 2005. Deglaciation of The Eastern Flank Of The North Patagonian Icefield And Associated Continental-Scale Lake Diversions. Geografiska Annaler, Series A: Physical Geography 87, 363–374.

Veres, D., Bazin, L., Landais, A., Toyé Mahamadou Kele, H., Lemieux-Dudon, B., Parrenin, F., Martinerie, P., Blayo, E., Blunier, T., Capron, E., Chappellaz, J., Rasmussen, S.O., Severi, M., Svensson, A., Vinther, B., Wolff, E.W., 2013. The Antarctic ice core chronology (AICC2012): An optimized multi-parameter and multi-site dating approach for the last 120 thousand years. Climate of the Past 9, 1733–1748.

Villa-Martínez, R., Moreno, P.I., Valenzuela, M.A., 2012. Deglacial and post-glacial vegetation changes on the eastern slopes of the central Patagonian Andes (47°S). Quaternary Science Reviews 32, 86–99.

Wenzens, G., 2002. The influence of tectonically derived relief and climate on the extent of the last Glaciation east of the Patagonian ive fields (Argentina, Chile). Tectonophysics 345, 329–344.

Wenzens, G., 2005. Glacier advances east of the Southern Andes between the Last Glacial Maximum and 5,000 BP compared with lake terraces of the endorrheic Lago Cardiel (49 degrees S, Patagonia, Argentina). Zeitschrift Fur Geomorphologie 49, 433–454.